J. Mater. Shaping Technol. (1987) 5:53–73

Thermomechanical Processing of Iron, Titanium, and Zirconium Alloys in the BCC Structure

D.L. Bourell and H.J. McQueen

Abstract. The body centered cubic (bcc) metals undergo a high level of dynamic recovery during elevated temperature straining so that the stress increases monotonically to a steady-state value σ_s. The strain rate and σ_s are related by means of the power, the exponential, or the sinh law with an Arrhenius temperature relationship. The activation energy for α iron has values of 250–280 kJ/mol, whereas for β titanium and β zirconium it is in the range 134–184 kJ/mol. The structure developed during hot working consists of elongated grains containing subgrains of dimension inversely proportional to σ_s. In warm working of α iron (limited to below 0.66 T_m), the textures are similar to those for cold working. In working β titanium and β zirconium which is limited to above 0.6 T_m except in β stabilized alloys or as matrix in $\alpha + \beta$ processing, the bcc textures transform into α textures. The α iron relies principally on substructure strengthening in association with carbides. The β phases can be thermomechanically processed to provide equiaxed or lamellar α in a variety of dimensions and combinations, with or without substructure. Hot working of the bcc refractory metal alloys, principally molybdenum, is similar to hot working of α iron.

INTRODUCTION

In the first two papers of this series [1,2] and in many other publications [3–17], the softening mechanisms during deformation, namely dynamic recovery and recrystallization, are explained. Dynamic recovery is the primary mechanism which reduces strain hardening and leads to a steady-state regime in metals such as α iron and aluminum [1,4,6,7,8]. It also bestows a high hot ductility insofar as it enhances accommodation of grain boundary sliding to inhibit triple junction cracking [2,6,9]. Dynamic recrystallization causes additional softening at high strains in certain metals such as copper, nickel, and γ iron [1,6,10,12] but is of minor importance in α iron. These mechanisms, which play an important role in traditional high strain rate hot working, are quite distinct from superplastic deformation which intervenes in specific temperature and strain rate ranges [17–26]. As will be described, the mechanisms of hot working often develop microstructures which are suited to boundary sliding, grain rotation, and switching.

D.L. Bourell and H.J. McQueen are with Concordia University, Department of Mechanical & Metallurgical Engineering, H36 IM8, Montreal, Quebec, Canada.

This paper is the third of a series of papers on hot working.

While the previous papers [1,2] discussed phenomena common to metals in general, this one on bcc metals, as well as others to follow on hexagonal close packed (hcp) and face centered cubic (fcc) alloys examines the occurrence and control of these phenomena in the processing of specific metals and alloys. The opening section examines the hot or "warm" working of ferritic iron alloys (bcc) which is quite distinct from hot forming of austenitic iron (fcc) because dynamic recovery plays a much more prominent role. Moreover, the industrial application of ferritic working tends to be mainly in near-net shape warm forging and limitedly in rolling, whereas in γ processing it is the other way around. The second section considers β titanium and β zirconium which are basically similar to bcc iron yet differ technologically because they are high temperature phases. The refractory bcc metals behave similarly to α iron but little has been published on their hot working. In each metal the discussion is extended to the combination of working with heat treatment in thermomechanical processing, to optimize specific service properties. Last, the behavior in creep [27–33] is occasionally referenced since it gives valuable insight into hot working behavior, especially where the latter is incompletely determined [14].

FERRITIC IRON ALLOYS

Deformation of α iron (α-Fe) and its dilute (bcc) alloys at elevated temperature is limited by the solid state transformation to fcc austenite, at or near 910° C ($\approx 0.66\ T_m$) [3,4,34–36]. However, when carbon is present in appreciable amounts, the maximum working temperature drops to about 720° C ($\approx 0.55\ T_m$). The transformation temperature may be raised considerably by additions of α stabilizers (aluminum, chromium, molybdenum, phosphorus, silicon, titanium, vanadium, tungsten). The common nomenclature for such high temperature deformation of ferrous metals is "warm" working with "hot" working reserved for higher temperatures, usually of γ iron, in which recrystallization plays a more prominent role. Dynamic recrystallization of α iron usually does not occur due to the high recoverability associated with the bcc structure.

As the temperature rises, the rate of strain hardening declines, particularly at high strain, until above 0.5 T_m, when stress–strain curves exhibit gradual monotonic hardening to steady-state regimes. The *constitutive behavior* of the non-work-hardening regime is marked by a decrease in flow stress σ with increasing temperature T and decreasing strain rate $\dot{\varepsilon}$ [4,36–41], which is modeled in one of these forms:

$$\dot{\varepsilon} = A(\alpha'\sigma)^n \exp(-Q/RT) \quad \text{[power law]} \quad (1)$$

$$\dot{\varepsilon} = A' \exp(\beta'\sigma) \exp(-Q/RT) \quad \text{[exponential law]} \quad (2)$$

$$\dot{\varepsilon} = A''[\sinh(\alpha'\sigma)]^n \exp(-Q/RT) \quad \text{[sinh law]} \quad (3)$$

where A, A', A'', α' and β' ($=n\alpha'$) are constants, R is the universal gas constant, Q is the activation energy, and n is the stress exponent. Solved for stress, these relations become, respectively,

$$\sigma = k[\dot{\varepsilon} \exp(+Q/RT)]^{1/n} \quad (4)$$

$$\sigma = 1/\beta' \ln [k'[\dot{\varepsilon} \exp(+Q/RT)]] \quad (5)$$

$$\sigma = 1/\alpha' \mathrm{Sinh}^{-1}[k''[\dot{\varepsilon} \exp(+Q/RT)]^{1/n}] \quad (6)$$

where k, k' and k'' are constants. The power law equation is applicable at low to moderate stress levels when dislocation glide/climb or grain boundary sliding is the rate limiting mechanism. The exponential model is valid at high stress (above power law breakdown, $\sigma \cong 10^{-3}E$), and is associated with the presence of excess vacancies. The sinh model, first proposed by Garofalo [42], is valid over ranges of stress both above and below power law breakdown. For plain carbon steels, additional empirical relations have been developed [43,44].

Figure 1 demonstrates the strain rate–stress relationship for α iron [27]. The activation energy was calculated to be 250 kJ/mole, which corresponds to

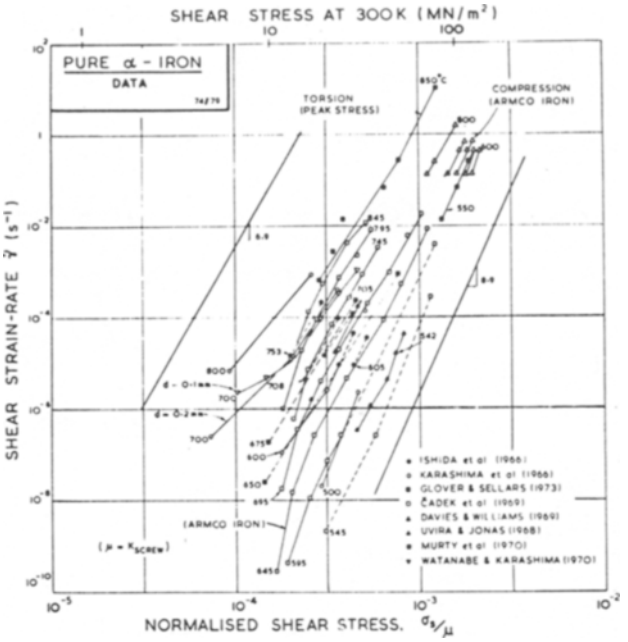

Fig. 1. Creep data for alpha iron at various temperatures. [ref. 27]

self diffusion of iron. The stress dependence of hot working may be described by the above equations using the temperature compensated strain rate, or Zener–Holloman parameter Z ($=\dot{\varepsilon} \exp [Q/RT]$). A limiting value of Z demarks dynamic recovery from dynamic recrystallization as the dominant restoration mechanism, recrystallization operating at Z values lower than the limiting value. For the case of commercial purity iron, the limiting value ranges between approximately $10^{12}s^{-1}$ and $10^{15}s^{-1}$, the larger values being applicable to higher purity material [36]. The activation energy is not strongly affected by impurity content and has been measured to be about 280 kJ/mole, compared to 250 kJ/mole for self diffusion.

Structure of Warm Worked α Iron

The *structural features* associated with warm working of α iron are subgrains [34,36,38–41, 44–49] with a low density of interior dislocations compared to cold working [50–56]. As temperature rises from ambient, α iron and its substitutional alloys (aluminum, chromium, nickel, silicon, manganese) exhibit higher levels of recovery as *subgrains* of increasing size and perfection [36–41,57]. In this respect, α iron is very similar to aluminum [57]. The addition of chromium [37,38,57–60] does not affect the subgrain size directly. Fe–25Cr torsion tested at 3.6 s^{-1}, 1050° C exhibits an elongated cell structure at low deformation which, upon continued straining, becomes equiaxed, 2 to 3 μm subgrains of low misorientation [57]. Eventually, a "super subgrain" structure develops, of 6 to 8 μm size and 3 deg to 13 deg misorientation, super-

imposed over the earlier structure. However, torsion testing of iron containing 0 to 20% chromium at 0.79 s^{-1} in the temperature range 600° C to 950° C produced identical subgrain structures at all strains independent of initial grain size and morphology, indicating that low chromium concentration does not alter fundamentally the restoration process [36,37]. Similar substructures have been observed in Fe–3Si [41,45,60], the subgrain size being independent of solute concentration.

Interstitial solute additions of carbon or nitrogen inhibit dynamic recovery in a narrow temperature band associated with dynamic strain aging [61–63]. In this "blue brittle" regime, solute-induced viscous drag of dislocations is responsible for the formation of an evenly distributed, dense dislocation structure and negative strain sensitivity. Additions of manganese expand the blue brittle temperature range to higher temperatures [61,62].

Impurities in α iron refine subgrains and increase strength with altered constants in equations (1) to (3). The strength increase has been associated wtih an increased drag on moving dislocations during hot working in the case of iron–chromium alloys [38]. Impurities also have a pinning effect on dislocations in the subgrain boundaries [64–65]. Gettering of impurities with elements such as titanium weaken subgrain boundaries, due to absence of boundary interstitials [60,64]. The presence of second phase dispersions of carbides of titanium [66] and chromium [38] hinder dynamic recovery and stabilize an augmented substructure density. The subgrain size developed at a constant flow stress is refined by the presence of carbides with small interparticle spacing.

Duplex subgrain structures have been reported during early stages of deformation [45], large subgrains present in grain interiors with fine subgrains near grain boundaries where compatibility imposes additional constraint. This is shown in Figure 2 for etch pitted Fe–3Si which was deformed 20% at 643° C. At high strains, the previously mentioned supersubgrain structure forms [58]. In plane strain processes microshear banding [60,67–71] and transition banding [68–70,72] produce substructure gradients.

The relation of the steady-state subgrain size d_s to the deformation parameters is written as

$$d_s^{-1} = B + C \log Z = (\sigma_s/k)^{1/q} \qquad (7)$$

where B, C, and k are constants and q varies between 1 and 0.5 [1,34,39,40,60]. The strain necessary to develop this steady-state subgrain size depends on the workpiece composition and processing parameters. Since alloys are generally stronger than pure iron, the dependence of flow stress on subgrain size is steeper

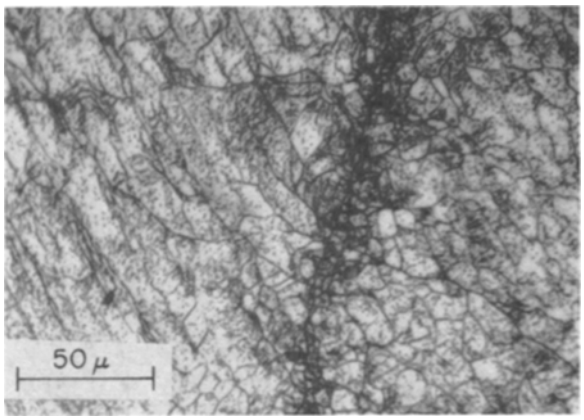

Fig. 2. Fe–3Si creep tested to 20% strain (643° C, 48 MPa) showing fine subgrain structure adjacent to the vertical grain boundary. [ref. 45]

for increasing alloy content [37,38]. An exception occurs in iron containing silicon above 800° C, in which silicon lowers the strength by increasing mobile dislocation density [41].

The steady-state *dislocation density* within subgrains ρ_s has been shown to bear a one-to-one correspondence with steady state subgrain size [51]:

$$\rho_s \alpha d_s^{-1} \qquad (8)$$

While this relationship has been established for warm worked austenitic steels in the temperature range of 600° C to 800° C, there is evidence that the same relationship is valid for ferritic alloys [41,46,61]. Because changes in subgrain size during processing are associated with changes in dislocation density according to equation (8), it has been difficult to separate the strengthening effects of bulk dislocations and the subgrain boundaries themselves. Kassner et al. [52,56] have shown by elevated temperature torsion and subsequent room temperature compression of γ stainless steel that subgrain boundaries account for about 10% of the strengthening effect, with major strengthening arising from dislocation interactions within subgrains.

In warm deformation as in cold, as long as recrystallization does not operate, the *grains* after axisymmetric elongation develop a fibrous appearance [48,73] and after plane strain are pancaked in the same ratio as the macroscopic shape change [74,75]. The contributions of grain boundaries to room temperature strength of the post-processed material depends on the extent of prior deformation. Figure 3 shows Hall–Petch curves for Armco iron worked at 500° C and at room temperature [76]. For both working temperatures increased straining lowers the slope of the tensile yield strength versus reciprocal square root of grain size plot, giving an indication that cold or warm strain harden-

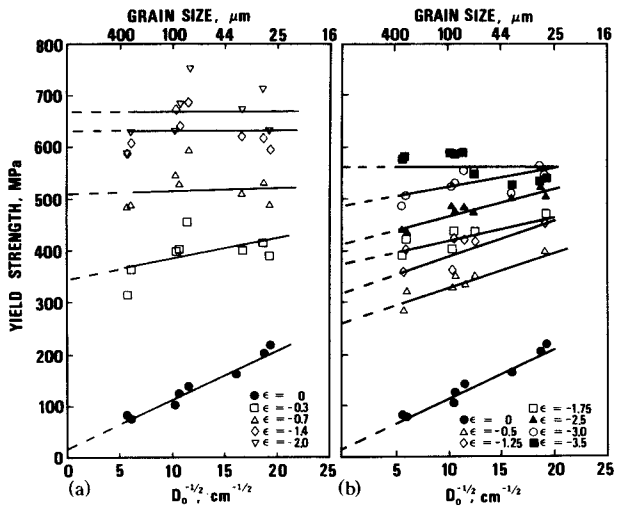

Fig. 3. Room temperature yield strength of Armco iron as a function of inverse square root of initial grain size (a) after room temperature deformation to various strains, (b) after warm rolling at 500° C (0.43 T_m). [ref. 76]

ing overshadows grain size strengthening. Dadras [77] has interpreted this to indicate that dislocations and subboundaries become the dominant barrier to free dislocation motion.

The *effect of warm working on the room temperature strength* of α iron is given by the

$$\sigma = \sigma_o + k_o d_s^{-p} \tag{9}$$

relation where $p \cong 1$ [34,40,48,60,64,78–80]. The term σ_o is sometimes rewritten $(\sigma_o' + k' D_o^{-1/2})$ to show explicitly the grain size contribution to strength [40]. Such substitution is balanced by evidence that subgrains 0.4 μm or smaller are more effective barriers to dislocation motion than grains of identical size [60]. Several empirical relations have been developed to incorporate grain and subgrain strengthening as well as extent of static recrystallization [81] and alloy concentration [43].

A microstructural feature associated with intermediate temperature deformation of pearlitic iron alloys is *accelerated spheroidization* of cementite [4,82–89]. This is evident in Figure 4 which shows the effect of torsional deformation on a eutectoid steel at 700° C. The eutectoid cementite deforms plastically and dissolves at regions of high disorder (subgrain boundaries and dislocations) to produce spherical particles. The flow stress declines markedly as spheroidization progresses and the substructure becomes more recovered. Cementite particles are smaller for larger Z, in association with smaller subgrains and higher flow stress [82–84, 86]. For constant conditions of testing, the volume fraction of carbide rises with carbon content

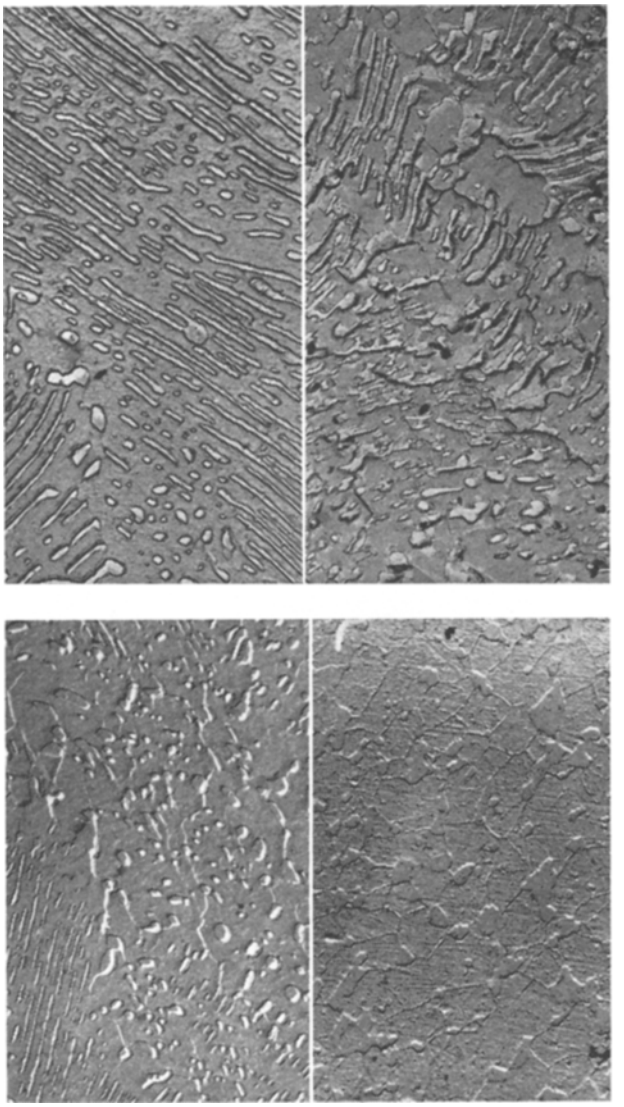

Fig. 4. Electron photomicrograph of a commercial grade eutectoid steel showing various stages of spheroidization as influenced by torsional deformation at 700° C and 2.4 × $10^{-2} s^{-1}$, 8000 ×. [ref. 85]

but the particle size remains constant [86]. At low strain rates ($3.0 \times 10^{-3}\ s^{-1}$) in a high purity eutectoid steel, the activation energy for accelerated spheroidization was found to be 178 kJ/mole, similar to the activation energy associated with static spheroidization [82,87]. Therefore, acceleration of spheroidization during hot working is not related to a change in mechanism from static annealing, but rather to an increase in the number of short circuit diffusion paths due to the introduction of a dislocation substructure. At high strain rates ($0.03\ s^{-1}$), accelerated spheroidization is enhanced by an increase in diffusivity associated with excess lattice vacancies.

Deformation during the transformation from aus-

tenite to ferrite in hypoeutectoid* steels (*continuum rolling*) results in grain refinement and carbide precipitation on subgrain boundaries, avoiding the formation of pearlite entirely [90–92]. This distribution of fine particles stabilizing a refined substructure leads to a higher strength and toughness than those of the pearlite and undeformed ferrite.

Isothermal hot working of ferrous metals in the $\alpha + \gamma$ *range* has been reported for the case of duplex stainless steels and carbon steels in the intercritical temperature range. In a duplex stainless steel at 900° C at strain rates up to 0.038 s^{-1}, the flow curves exhibit monotonic hardening to strains of 0.5 with both phases undergoing dynamic recovery [93,94]. Only at 0.38 s^{-1} does the austenite undergo dynamic recrystallization causing a peak in the flow curves. The ferrite exhibits a high degree of dynamic recovery. It is possible that at lower strain rates the ferrite carries a larger share of the strain so dynamic recrystallization is not triggered in the austenite [93]. Similar results have been obtained for FERRALIUM 255 duplex stainless steel at low (0.05 s^{-1}) and high (5 s^{-1}) strain rates in the temperature range 950° C to 1100° C [95]. In a duplex stainless steel studied across the entire range of phase fractions, the flow stress was lower than the law of mixtures and even showed a minimum near 75% α [96]. Examination of the grains of the two phases indicated that the ferrite carried significantly more strain at a fraction of 30%. At higher fractions, both phases carried less than the average strain as a result of enhanced grain boundary sliding. This effect appears to be the closest that $\alpha + \gamma$ mixtures come to superplastic behavior, which is in contrast to that in $\alpha + \beta$ titanium or zirconium alloys to be described later.

A study on a carbon steel showed that the flow stress of an $\alpha + \gamma$ mixture depends on the shape of the phases [97]. In equiaxed $\alpha + \gamma$ produced by heating up into the two-phase region, the flow stress falls below the value of a mixture and close to the value of the ferrite. In a structure produced by cooling such that the ferrite occupied austenite grain boundaries, the stress was much higher. This was true at 70% ferrite, but on heating from 800° C to 825° C where the ferrite content is about 30% there is not a difference in stress on heating or cooling. This occurs because the ferrite is no longer able to assume a larger portion of the strain.

Hot Ductility of α-Fe

A brief statement on *hot ductility* is needed to clarify the diverse effects of various testing methods and initial microstructures. Failure in forming depends strongly on the stress state induced and this is reflected in testing [2,9]. Tension, because of necking, gives an underestimate of ductility compared to process behavior; torsion, being pure shear, gives an overestimate and compression often provides no information when it is limited to uniform strains without hoop cracking. The cast structure usually exhibits low ductility because of segregation and coarse grains and may vary widely with location in the ingot. However, once the cast macrostructure is broken down by one or two stages of 30–50%, the homogenous, equiaxed worked structure exhibits much higher ductility (which is the behavior reported later), usually of 60–100% tensile elongation and torsional true strains of 10–100. The mechanisms of failure usually include grain boundary sliding, cavitation, and triple junction cracking which may be drastically enhanced by segregated solutes or phases [2,9]. In addition to these, superplastic behavior can give rise to good workability, notably elongations of 100–800%, with failure possibly due to cavitation [17–26].

Improvements in ductility by hot working ferritic alloys arise from several sources. Outside the blue brittle regime, additions of up to 0.01 carbon increase the ductility by reducing the volume fraction of oxide particles, but if more than that, decrease it as the volume fraction of carbides rises [86]. The ductility rises remarkably at high temperatures, because the highly recovered grains are able to accommodate grain boundary sliding [9]. In Fe–25 Cr, torsional ductilities of between 200 and 650 have been obtained in the temperature range 900° C to 1000° C [98–101] although it is reduced significantly at slightly lower temperatures by trace impurities, principally oxygen [38]. Additions of aluminum [66] and manganese [61,62] do not affect ductility greatly. An exception is Fe–8Al at temperatures near 700° C, in which grain boundary cracking occurs [66]. Termed red shortness or a mid-range ductility minimum, this phenomenon is extended to lower temperatures by additions of up to 5% nickel. Nickel additions greater than 5% produce embrittlement over the range 500 to 800° C. The crack initiation in Fe–8Al caused by localization of deformation at grain boundaries [101] can be eliminated through addition of fine second-phase particles such as titanium carbide [66]. When chromium or nickel are present, addition of manganese extends the blue brittle range by about 100° C [61,62].

Upon heating, *austenite* is formed, initially in association with segregation at grain boundaries. The ductility of the multi-phase iron decreases rapidly due to the presence of hard γ particles [4,37,41,86,102–104]. Minimum ductility occurs at about 80% austenite which has only one-half to one-third the ductility of ferrite [4,37,41]. At a common temperature the strength of γ is higher and its ductility is lower than

*Carbon concentrations lower than the eutectoid composition of approximately 0.8%.

those of α because of the lower self diffusivity and stacking fault energy of the fcc lattice [4,37,41,86,103]. A similar behavior is found in mixtures of δ and γ iron except that the effects appear on cooling. As the carbon content increases, the ferrite's ductility is diminished by the increasing cementite fraction so that at 0.4% carbon the ductility below the transformation temperature equals that above it of the γ phase which is enhanced by the carbon in solution. For higher carbon contents, the austenite is more ductile than the ferrite [86].

Billet geometry appears to play an important role in formability in the warm working range. For the case of rolling, Schey [105] has predicted that "alligatoring" fracture, separation parallel to the rolling plane, occurs when the ratio Δ of the billet thickness to the roll contact length equals two. Sherby et al. [106] measured this ratio as a function of warm rolling strain for AISI 1020 steel rolled at 5 to 10% reduction per pass at room temperature and 500° C. The critical value of Δ was two for rolling at room temperature, but decreased towards unity as the temperature increased to 500° C, Figure 5. While this type of fracture behavior arose from residual stresses from the deformation processing, the structural dependence of rolling plane fracture has not been established. In Hypereutectoid steels rolled to large pass reductions at 300° C to 500° C, wavy crack "unzippering" separates the billet on a plane containing the rolling direction and the thickness direction [106]. In addition, "edge cracking" associated with secondary tensile stresses is relatively common in warm rolling of α-Fe alloys.

Texture Effects

Because extensive recrystallization does not occur during most warm working, crystallographic textures develop [81,107–116]. For small strain, isothermal, multiple pass deformations, the texture development is similar to that observed during room temperature deformation. This development has been described by Dillamore and Roberts [107] to be initially (112)⟨110⟩, which gradually shifts toward the (100)⟨110⟩ texture. This has been observed by several investigators [117–119]. For the case of total rolling reductions as large as 98%, the intensity of (100) poles parallel to the short transverse direction has been shown to increase linearly with rolling strain independent of temperature in the range of 590° C to 650° C [115]. When the deformation is imposed as a single pass, a different type of texture develops. Hawkins [109,114] has shown for low carbon steels rolled at 600° C to strains of approximately 1 that a texture forms with (100) poles parallel to the short transverse direction but with otherwise random orientation, Figure 6. For axisymmet-

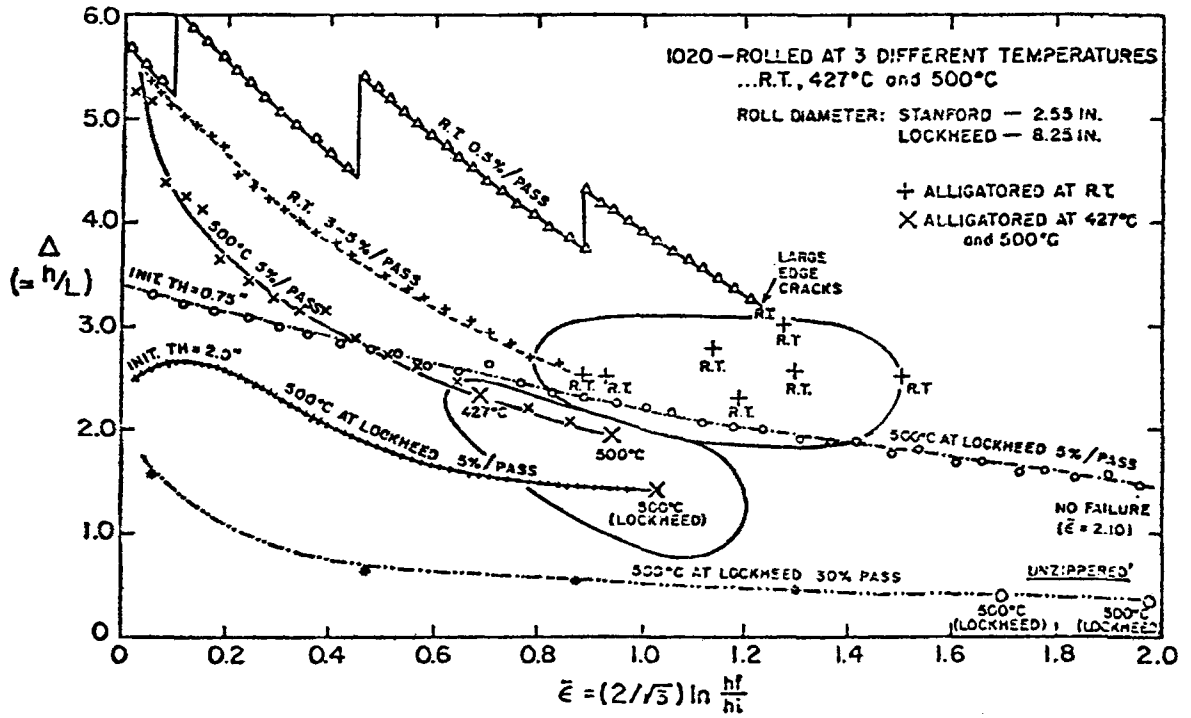

Fig. 5. A plot of the ratio of the billet thickness to roll contact length for multiple pass rolling of mild steel. Failure by alligatoring occurs within circled regions on the plot for cold and warm rolling. Alligatoring can be prevented by avoiding these regions, as can be noted by the lines extending to mean strains of two. [ref. 106]

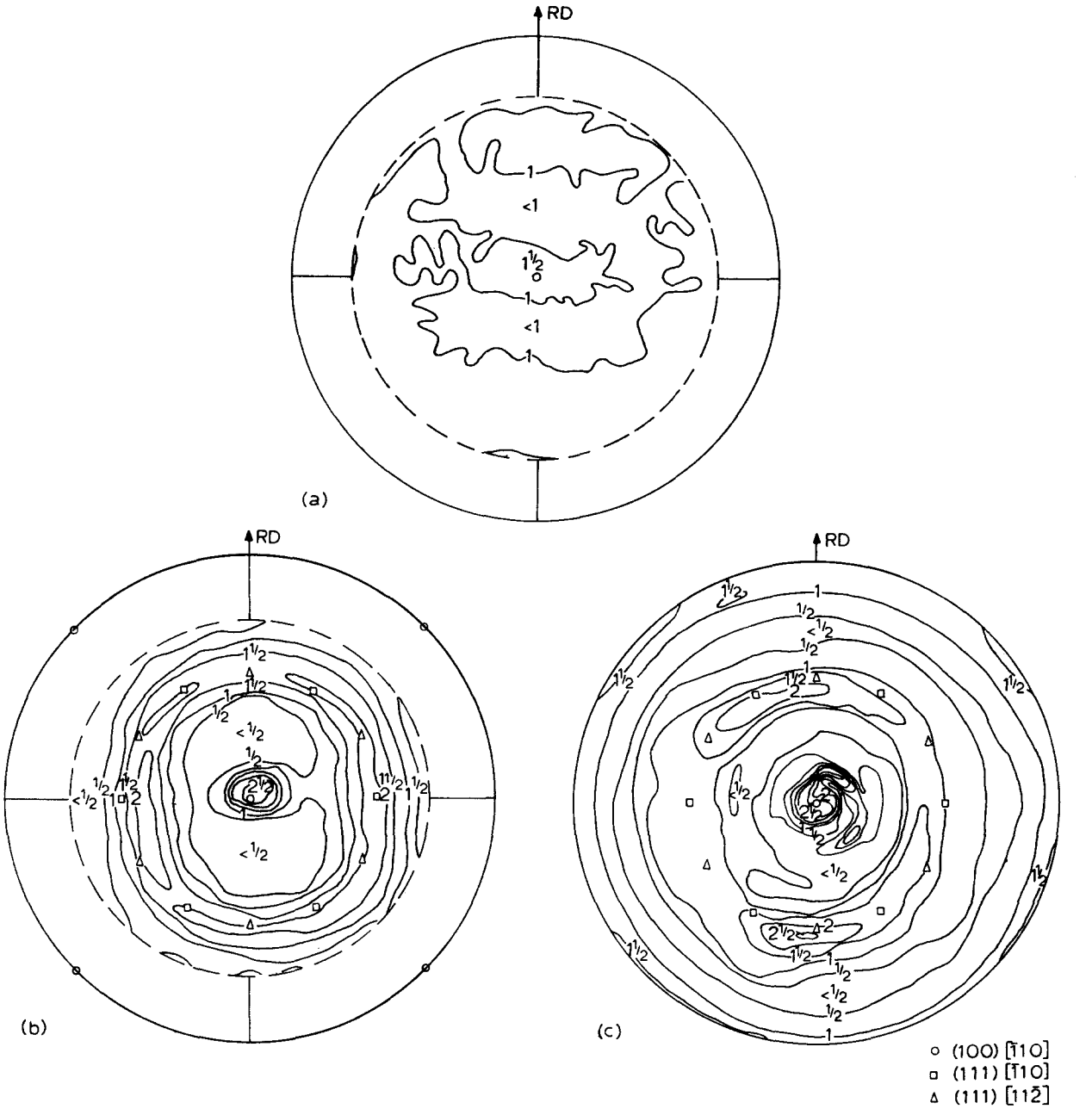

Fig. 6. (200) pole figures for mild steel of two carbon contents rolled at 650° C in a single pass to a thickness strain of 0.96. (a) as hot worked, (b) 0.11% carbon, (c) 0.017% carbon. [ref. 114]

ric extrusion of low carbon steel with ratios of 5 to 10, the ⟨110⟩ fiber texture developed at 660° C is identical to room temperature deformation [120–122].

Bramfitt and Marder [81] investigated the textures developed in a hot rolled 1.05 manganese steel containing less than 0.002% carbon. The steels were rolled under continuous cooling conditions, and the total strain accumulated below the intercritical range increased with decreasing finishing temperature between the eutectoid temperature and 150° C. The texture of the finished steel was of the (111)⟨110⟩ type, and the intensity increased as the finishing temperature decreased, Figure 7.

Recrystallization

In highly purified irons, the high mobility of the grain boundaries gives rise to *dynamic recrystallization* despite a high degree of recovery [36,38]. Dynamic recrystallization occurs when Z is less than a limiting value which is composition dependent. Alloying de-

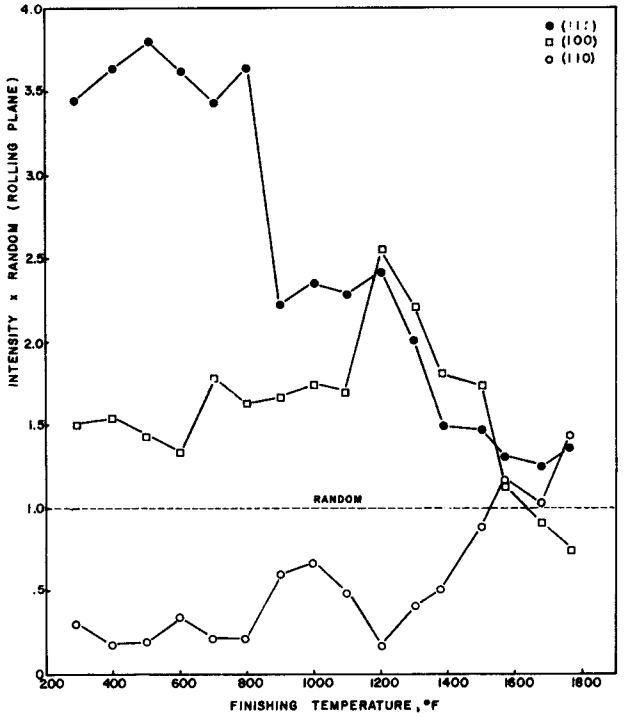

Fig. 7. A plot of intensity of (111), (100), and (110) poles as functions of finishing temperature for 1.05Mn–0.002C steel rolled under continuous cooling conditions through the intercritical temperature regime. [ref. 81]

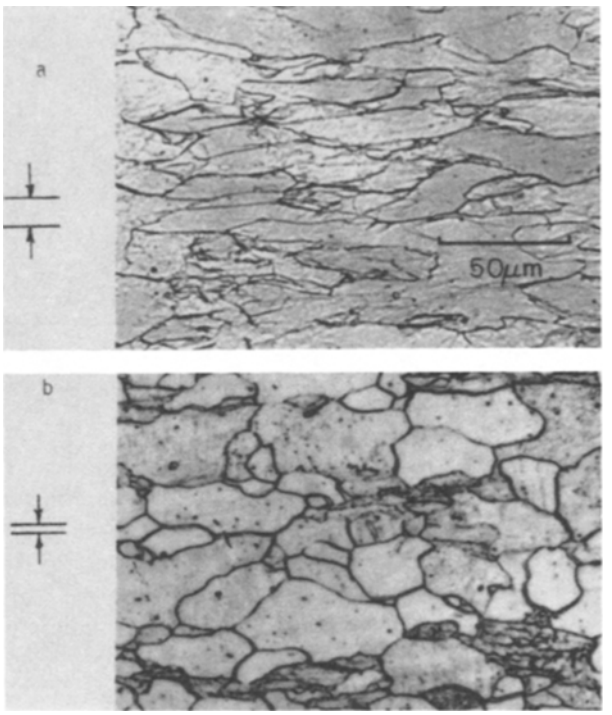

Fig. 8. Influence of rolling at 600° C on the transverse grain structure of Armco iron deformed to thickness true strains of (a) −1 and (b) −2. Unlabeled distance markers to the left of each micrograph indicate the predicted grain dimension assuming no recrystallization. The large discrepancy between this dimiension and grain size in (b) is indicative of recrystallization. [ref. 74]

creases the limiting value of Z, thereby inhibiting dynamic recrystallization. In iron, the activation energy for dynamic recovery and dynamic recrystallization is about 280 kJ/mole whereas it was 253 kJ/mole for self diffusion and 294 kJ/mole for static recrystallization [36].

When deformation takes place by multiple passes with significant hold times between passes, static recrystallization must be considered as well. This is illustrated by Figure 8, which shows microstructures of Armco iron rolled at 600° C to total reductions of 63% and 86% in multiple passes, with 5 minute interpass anneals [74]. The lower strain material does not show recrystallization, but the other material is almost recrystallized. The mean value of Z for the deformation has been calculated to be $6 \times 10^{16} s^{-1}$, much higher than the limiting value of Z for even high purity iron. For this reason, it is unlikely that the recrystallization shown in Figure 8b is dynamic.

Static recrystallization between passes in multistage hot rolling is important in refining the structure and lowering the flow stress in the following pass [11,15]. Compared to γ-Fe processing, α-Fe is likely to exhibit more recovery and less recrystallization for a given interval, partly because of the reduced operating temperature and partly because of its much higher recoverability both in the previous working and in the hold period.

The interrelation between dynamic and static recrystallization in α-Fe has been advanced considerably by a number of investigators by use of interrupted hot compression or torsion testing [123–125]. Generally, static recrystallization after hot working in the dynamic recovery regime is similar to that after cold working. The time for recrystallization is reduced by increasing the temperature and strain. In dynamically recovered Fe–3Si, nucleation sites for static recrystallization were grain boundaries and inclusions [125]. The growth rate of newly formed grains was found to be inversely proportional to hold time and independent of temperature and strain. This contrasts with high purity irons, in which time-independent growth rates was measured [124]. The recrystallization behavior of dynamically recovered low carbon steel is similar to that of high purity iron [123].

After hot working in the recrystallization regime, *metadynamic recrystallization* proceeds through the growth of existing recrystallization nuclei formed im-

mediately prior to cessation of deformation [123,124]. For this reason it takes place without an incubation period. As these nuclei grow into material which is heterogeneously strained, the growth rate decreases with time [124]. Under certain circumstances, classical recrystallization may also occur, associated with nucleation at high energy sites followed by subsequent growth [123]. For both dynamic and static recrystallization, the grain size is inversely proportional to $(\text{stress})^{2.2}$, independent of temperature [124]. Metadynamic grain size is usually larger than the grain size from which it forms [124].

Applications

The primary reason for warm forging [35,126–132] is a *reduction in manufacturing costs* associated with lower heating requirements and conversion from hot forging to a near-net-shape process. To be specific, warm working produces less oxidation [128,133–135], less shrinkage [136], and improved dimensional tolerances [128,133,136–140]. Warm working has been considered superior to cold working in reducing press loads [89,128,133,136,141–144] and enhancing void closure [145]. Moreover, improved productivity results from elimination of both preparatory treatments [128,134,146] and interpass or post-working heat treatments [128,136,147–149] and even environmental accommodation of robots [150].

The warm working regime has also been used as the processing range for ferritic materials which exhibit superplasticity [17,151–154]. Superplastic behavior in iron–carbon alloys demands fine grained ferrite and a fine dispersion of spheroidized cementite to inhibit grain growth. The carbon content ranges between 1.3 to 1.9%. By repeated rolling at decreasing temperature from γ through the transformation to α, adequate grain boundary stabilization is achieved by carbide spherules. Upon heating to 650° C, Walser and Sherby [152] obtained elongations as great as 760% in 1.6 carbon steel strained at $6.7 \times 10^{-5} s^{-1}$. These steels also exhibit γ phase superplasticity but have lower ductility due to dissolution of some stabilizing iron carbide [151,152].

Primary processing of ferritic iron to produce *improved properties* is another area of interest. Rolling, extrusion, and drawing have been focused areas. Improvements in ductility and toughness at a given strength level compared to cold working are the main advantages [46,47,49,76,77,136,146–149,155–164]. This is illustrated in Figure 9, a plot of the percentage of elongation versus 0.2% yield strength for cold and warm rolled Armco iron [76].

The impact behavior of warm worked ferritic iron has received considerable attention due to an interesting delamination fracture mechanism. Figure 10 shows the impact energy measured as a function of test temperature for a 2.1 manganese–2.9 chromium HSLA steel which was controlled rolled to a finishing temperature of 750° C and with 80% of the reduction below 800° C [165]. The salient features of delamination fracture are a broadened transition region instead of the usual sharp drop associated with the shift from a ductile failure mode to transgranular cleavage, and secondary cracking normal to the main crack plane. The transition broadening is due to splitting in the plane of the sheet a a result of texture [108, 109, 111–116], inclusions [126,166–171], grain boundary separation [81,110–112,172], and elongated prior austenite grains [167].

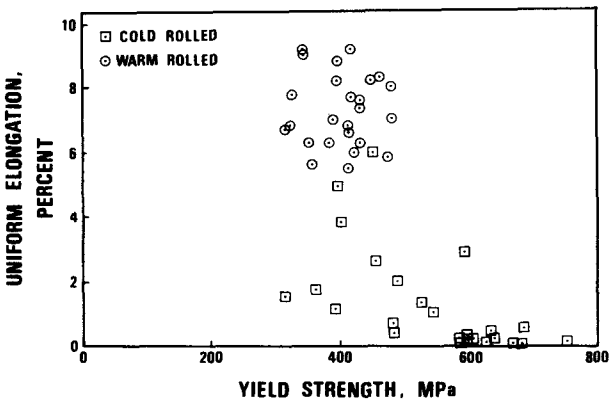

Fig. 9. Room temperature ductility of cold and warm (500° C) rolled Armco iron as a function of yield strength. [ref. 76]

TITANIUM AND ZIRCONIUM IN THE β BCC PHASE

These two metals are highly similar in having bcc phases above 0.59 T_m (titanium) and 0.55 T_m (zirconium), and at lower temperatures, hcp phases which because of low c/a ratios ($\sim 1.59 < 1.633$ ideal), undergo both basal and prismatic slip. This produces relatively good formability and structural toughness. With appropriate solute additions, alloys of α, $\alpha + \beta$ or β phases may be stable at room temperature. Their common alloys are quite different because titanium is applied principally for strength, toughness, and fatigue resistance in low to medium temperature aerospace service, whereas zirconium must have good creep resistance and low neutron cross section for nuclear applications.

Because the β phases are softer and more ductile than the α, hot working may be undertaken in either α, $\alpha + \beta$ or β condition. The working temperatures

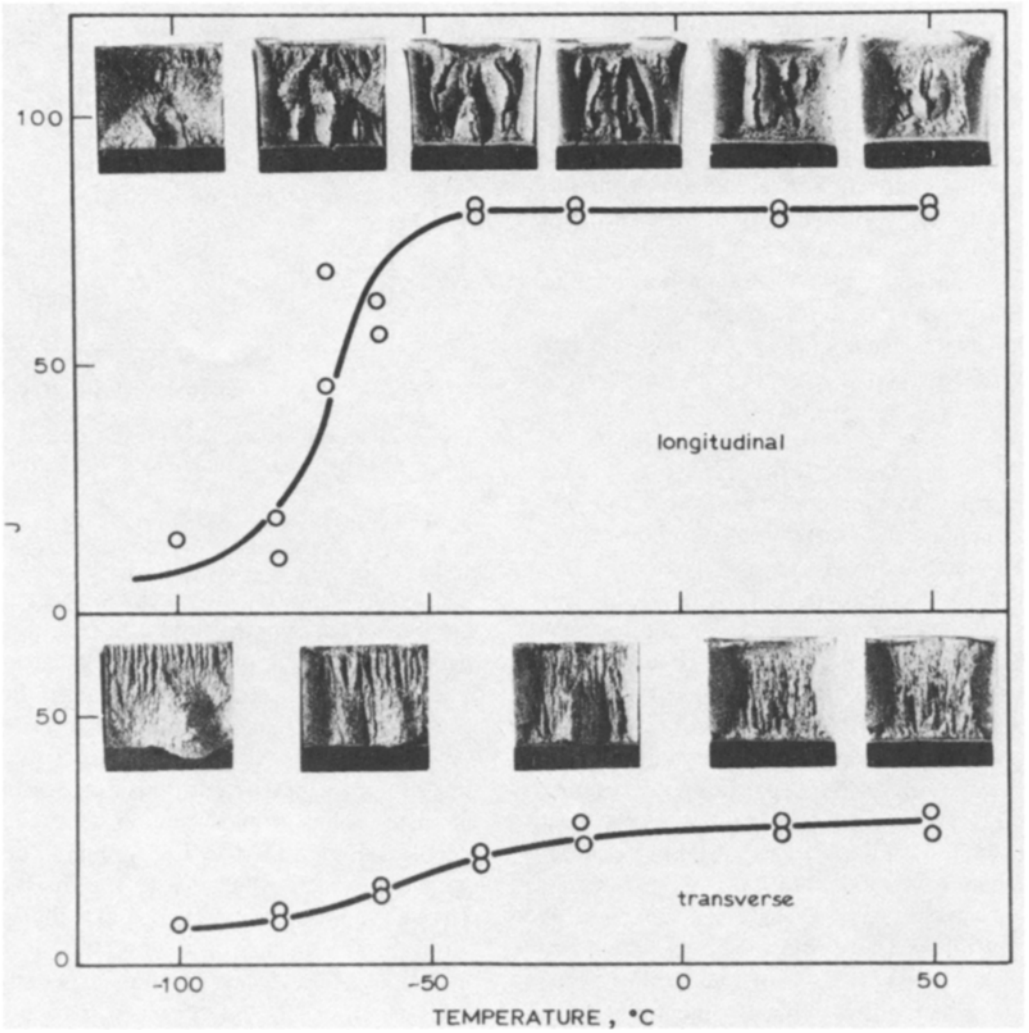

Fig. 10. Impact transition curves and fracture appearance of longitudinal and transverse Charpy-V specimens of 2.1Mn–2.9Cr HSLA steel controlled rolled to a finishing temperature of 750° C. [ref. 165]

and strains may be combined with intermediate or final heat treatments in thermomechanical processing to produce structures with optimized properties; these will be discussed in the later review devoted mainly to the hcp phases. Here the deformation of β phases are described, compared and contrasted with α-Fe. The working of $\alpha + \beta$ alloys are considered briefly in so far as it is related to the behavior of the β phases. The α phase, being stable at low temperatures and stronger than β, plays a role somewhat like cementite in ferritic steels; however, it may appear as retained primary phase α_p (equiaxed at grain boundaries, GB), as precipitated GBα, or as Widmanstatten matrix precipitates (but never as eutectoid plates). While the α is inherently more formable than the carbide, it often reaches much higher volume fractions as the temperature decreases and its different crystal structure and texture make slip transfer from β difficult and induce anistropy.

Deformation of β Titanium Alloys

In the hot deformation of bcc β titanium alloys, the *flow curves* exhibit a *monotonic increase to a steady-state regime* Figure 11a, [173–177]. The β phase is softer for a given Z than the α phase [27,28,178], having a lower power-law exponent ($n = 4.0$) (Figure 11b) and a much lower activation energy in the range 137 [177], 153 [28.177], and 171 kJ/mol [179] as compared to 185–242 kJ/mol [27,28,176,178]. This reflects the rapid diffusion rate in the β, which is about two orders of magnitude higher than other bcc metals (Q_D = 153 kJ/mol, about one-half normal for bcc) [27,28]. Rapidly cooled microstructures consist of elongated grains with well-developed substructure [173,180–184]; slow cooling leads to static recrystallization [183]. The hot worked substructure develops more strongly near the grain boundaries and spreads inwards; it is fairly resistant to recrystallization,

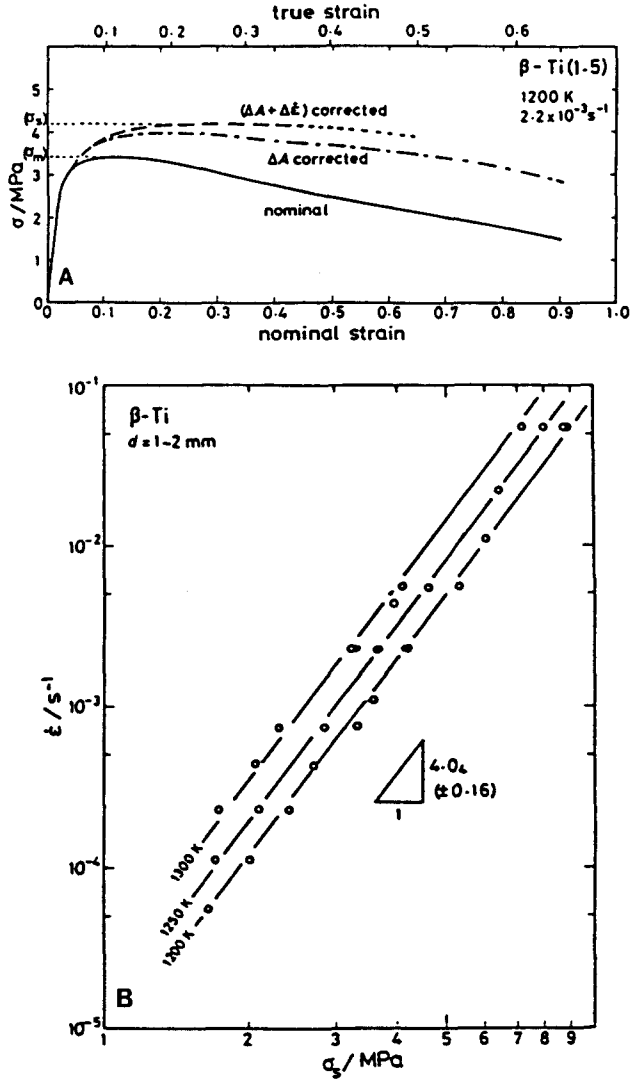

Fig. 11. (a) A flow curve of beta titanium tested in tension at 1200° K and 2.2 × $10^{-3}s^{-1}$, showing corrections for the reduction in cross-sectional area and for changes in true strain rate. (b) The stress–strain relationship for beta titanium between 1200° K and 1300° K. [ref. 177]

undergoing static recovery at the forming temperatures as in other bcc alloys. Static recrystallization usually starts near the grain boundaries, or at shear bands, but goes to completion very slowly because of static recovery of the interior. Static recrystallization is enhanced by high strains and by annealing temperatures above that of deformation [185,186]. This microstructural evidence indicates that the observed peak stress and work softening likely arise from structural changes other than dynamic recrystallization.

Working of Titanium α + β Structures

In the hot deformation of α + β structures at high $\dot{\varepsilon}$, both the α [187] and β [180,188,189] become elongated and develop substructures and independent textures. When α particles are isolated within large β grains, the behavior is essentially that of β phase with increased flow stress due to the hard α [190]. For equiaxed α and β, in alloys such as Ti–6Al–4V [190,191] and Ti–6Al–2Sn–4Zr–2Mo–0.1 Si, the flow stress rises to a steady-state plateau and the activation energy is about 150 kJ/mol similar to β phase [180,186,189,192]. However, similarly deformed lamellar α + β (air-cooled β) exhibits a peak with work softening to the same plateau as the equiaxed α + β under the same conditions [192,193].

Lamellar or Widmanstatten α in a β matrix is refined by segmentation during deformation and annealing at 950° C; the aspect ratio can be reduced from 20 to 3 by strains of about 1 [181,189,193,194]. The α plates are divided along their length by either shear bands with large misorientations or by subboundaries. Annealing leads to static recovery and β phase penetrates down the low angle boundaries and separates plates up to 7 μm thick (Figure 12) [186,194]. This mechanism has much similarity to the spheroidization of cementite in warm worked pearlitic steels; however the cementite plates are less formable and are in much lower, constant volume fraction.

Superplasticity and Hot Ductility

When the equiaxed α + β structure is very fine, deformation at strain rates below 10^{-2} s^{-1} gives rise to an almost unelongated structure [190,193,195–197] accompanied by high values of strain rate sensitivity m and large elongations [179,197–199]. This superplastic behavior is associated with a strength about one-third that of normal material. However, substructure and high work hardening rates are often observed, especially at higher strain rates [197,198]. Superplasticity, as found in Ti–6Al–4V and Ti–5Al–2.5Sn, is

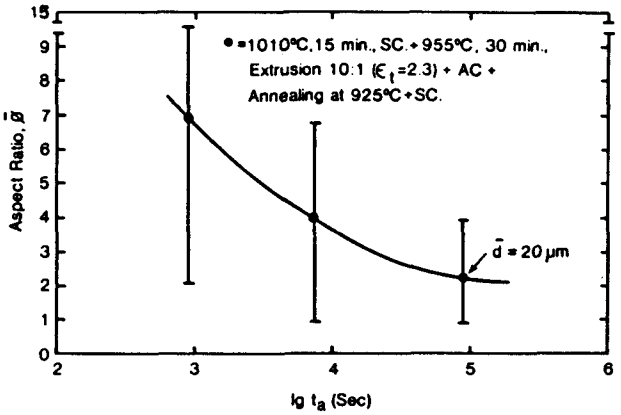

Fig. 12. Effect of post extrusion annealing time on the mean and range of aspect ratio values of coarse alpha plates in titanium. [ref. 194]

limited to the $\alpha + \beta$ region and is enhanced where β volume fraction and diffusivity are high [23,24,200]. In the β regime (Ti–8Mn, Ti–15Mo, Ti–13Cr–11V–3Al), superplasticity is found in association with subgrain formation, grain boundary serrations, and grain pinching off under conditions of strain rate cycling up into the dislocation creep regime [24].

The *hot ductility* of titanium alloys is very high in the *β phase* with tensile elongations of 90–100% (Figure 13) [174,175]. The ductility is unaffected by cooling rate and by strain rate between 1.5 and 25 s^{-1} which likely represents the peak range. The mechanism is ductile with almost no grain boundary cracking. The ductility diminishes to 30% on cooling into the $\beta + \alpha$ *transformation region* (Figure 13) [174] as a result of intergranular fissuring, which usually nucleates at interfaces with GB α. The fracture becomes entirely blocky; however, the faces have small dimples indicating localized flow in the β phase [175]. On the other hand, the ductility of $\alpha + \beta$ is usually very high when the structure is more refined, the temperature near 700° C and the strain rate low to give to the superplastic regime [180].

One *industrial objective* of β hot working is the production of *uniform, fine grains*. Working to small strains ~30% tends to give substructure gradients from edge to center of the grains so that recrystallization initiates at old boundaries but does not progress into the low density dynamically and statically recovered regions [185,186]. At low temperatures, nuclei also form on shear bands. A "processing window" for refining Ti–10V–2Fe–3Al alloy consists of working in the range 705–1365° C followed by annealing at higher temperature after working at either end of the T range or at lower strains for larger initial grains [185,186]. The β alloy, Ti–15V–3Cr–3Al–3Sn, has the advantage that it can be continuously rolled in the β phase whereas the $\alpha + \beta$ alloys, such as Ti–6Al–4V, must be pack rolled on a hand mill with reheating [201]. Because of its bcc structure the sheet can be produced with almost no in-plane anisotropy and with excellent cold formability. Nominally β alloys usually precipitate α particles which are utilized for strengthening. In both β and $\alpha + \beta$ alloys *working of β through the transformation* has beneficial effects on toughness by eliminating GB α since homogeneous sites are enhanced [188]. In metastable β alloys, high temperature working also precludes formation of ω phase and leads to direct nucleation of α particles on dislocations to improve the ductility and toughness [188]. The working of β alloys with about 0.1 volume fraction of primary α_p leads to equiaxed α which has much higher ductility for a given strength then either a higher level of α_p or GB α which leads to strain localization [28]. The varied strength levels are obtained by heat treating to control the intragranular α precipitate.

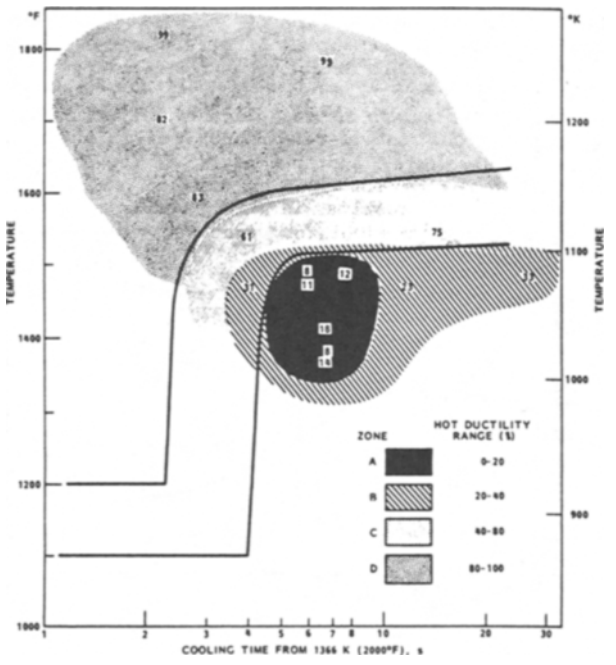

Fig. 13. On-cooling hot ductility of Ti-6211. The hot ductility shows a minimum centered at 1400° F and at a cooling time from 2000° F of 6 seconds. [ref. 174]

Hot Working of β Zirconium

The creep rates are much higher in β phase zirconium (Zr) than in α, as in titanium [28]; at the $\alpha - \beta$ border on a deformation mechanism map, they rise abruptly because β phase exhibits power-law creep with n = 4.3 and Q_C = 184 kJ/mol compared to n = 6.6 and Q_C = 271 kJ/mol for α. Surveyed stress creep data for 970–1600° C (Figure 14) confirms the suitability of a dislocation climb model and a power law equation with n = 3.8 and Q_C = 142 kJ/mol (individual values range over 134–188 kJ/mol) [179,202].

Hot compression results for β-Zr have been analyzed by the sinh relationship of equation (3) with n of 3 and Q of 142 kJ/mol [179,203]. The hot compression curves at 1000° C at 0.15 s^{-1} for both Zr and Zr–2.5Nb (niobium) exhibit strain hardening to plateaus of 10 and 20 MPa, respectively (Figure 15) [204,205]. This can be compared with an extrapolated strength of about 25 MPa for α-Zr [207]. The n for steady-state stress if 4.0 for Zr and 4.2 for Zr–2.5 Nb (Figure 16a) [204,205]. Zircaloy-2 (1.5Sn–0.13Fe–0.1Cr–0.5 Ni) has n between 3.6 and 4 and an activation energy of 143 kJ/mol [207]. With addition of 12,000 ppm O, the behavior is little changed but the strength increases in proportion to exp [0.34 (% 0)] in comparison to exp [0.57 (%O)] for α. The tests showed that the activation energy varied from 120–150 kJ/mol and n from 3.1 to 3.7 [207–209]. The first stage in production of Zr–2.5Nb *pressure tubes* is β upset-

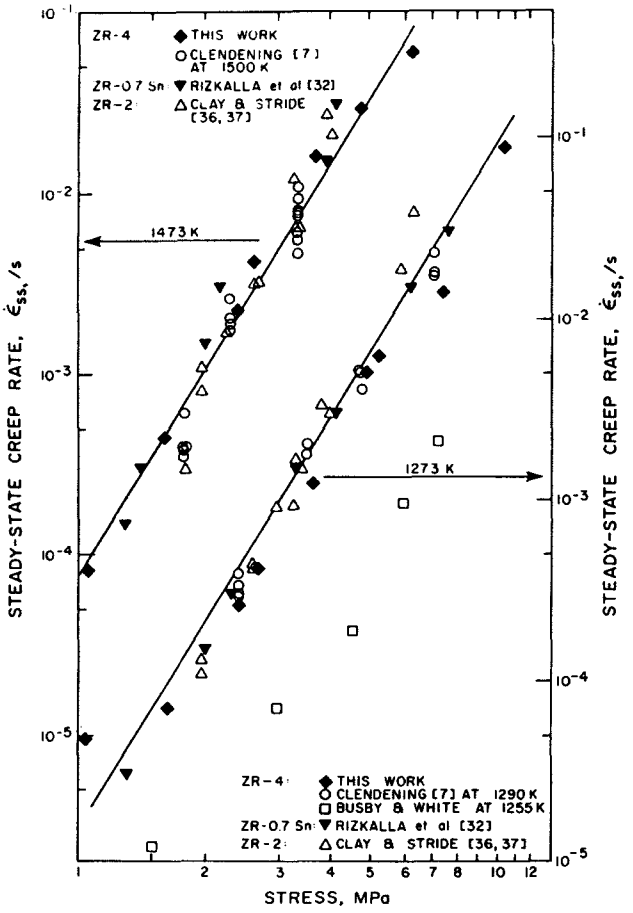

Fig. 14. Steady-state creep rate versus applied stress for tests conducted on beta zirconium at 1273° K and 1473° K. [ref. 202]

ting of ingots followed by rapid cooling to refine the α phase.

Alloys with niobium contents of 10, 15, and 20% were examined to determine the properties of the metastable β phase in 2.5 Nb alloys. At 925° C, 1.5 $\times$ $10^{-3}s^{-1}$, the strength of 10 Nb is about 40 MPa compared to 10 MPa for 2.5 Nb [205]. The curves show a definite strain softening (Figure 15b) which is thought to result from the disintegration or overaging of Nb clusters which form as a result of the miscibility gap. No dynamic recrystallization is observed. This analysis is supported by the rise in strength resulting from annealing between stages of deformation, which reforms the clusters; this varies from 50% increase at 825° C to 10% at 1025° C [205]. *Alloys with 2 to 6% molybdenum* are 4 to 8 times stronger than β-Zr at strains at 0.7 (Figure 16b) [210]. They exhibit anomalously high yield stresses as a result of formation of an α layer due to oxygen contamination; flow softening takes place as slip destroys the effectiveness of the layer.

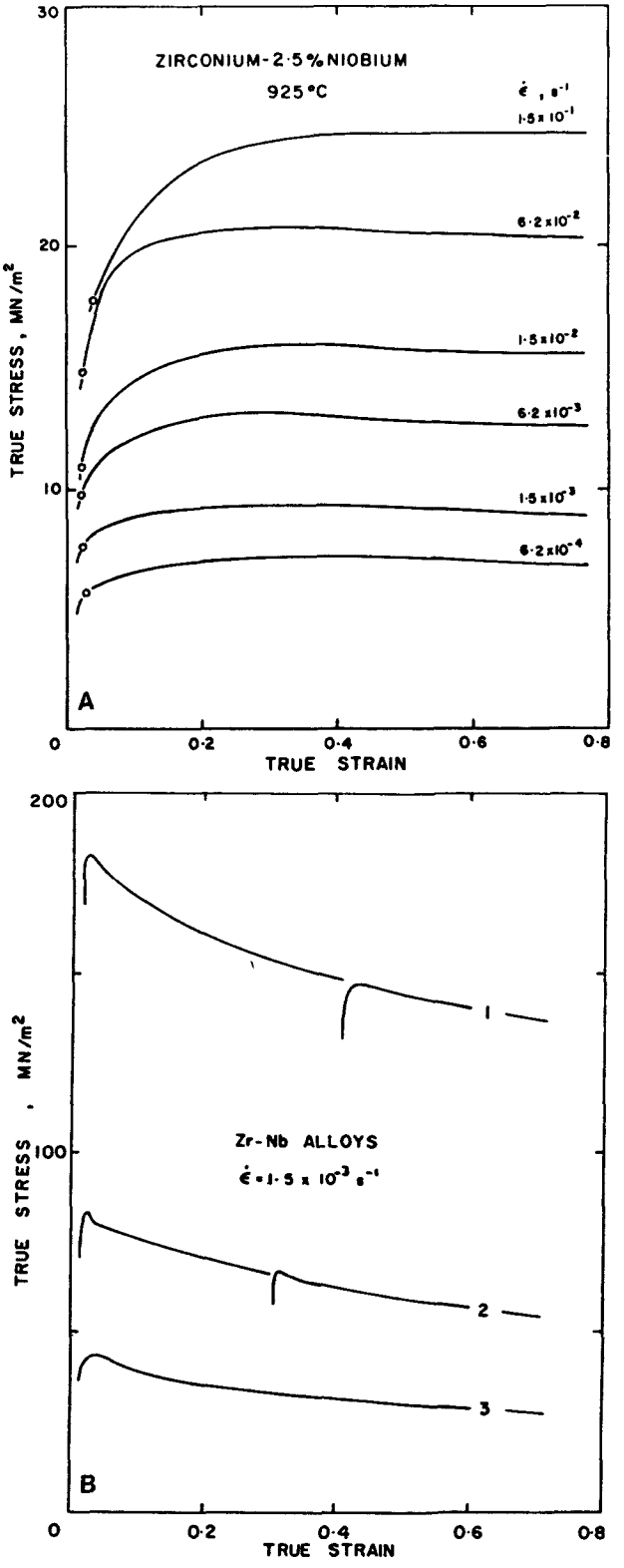

Fig. 15. Flow curves for Zr–Nb alloys. (a) Compression test results for Zr–2.5Nb at 925° C, circles representing the 0.2% offset yield stress. (b) Flow curves for higher Nb alloys showing marked flow softening. Curve 1: Zr–20Nb, 725° C; interruption delay—10 minutes. Curve 2: Zr–15Nb, 825° C; interruption delay—30 minutes. Curve 3: Zr–10Nb, 875° C. [ref. 205]

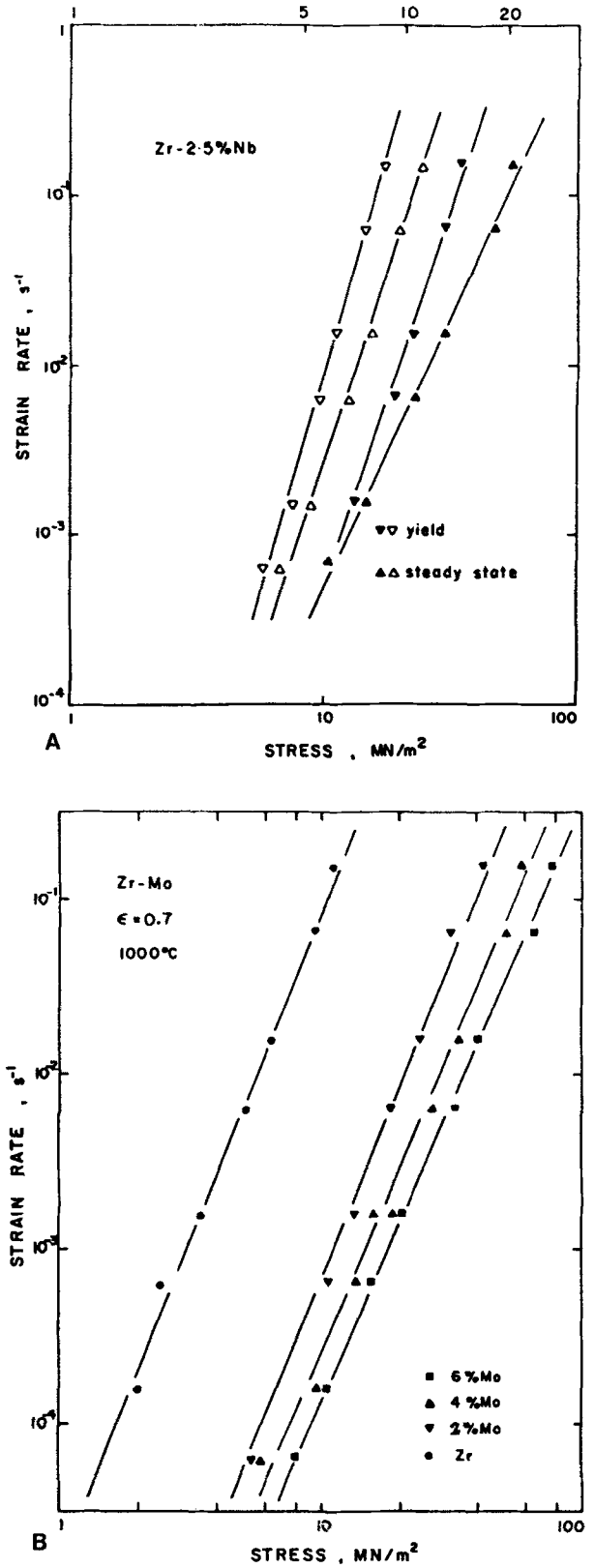

Fig. 16. Strain rate dependence of stress for (A) Zr–2.5Nb at 925° C (open symbols, lower scale) and 1025° C (closed symbols, upper scale), and (B) Zr–Mo at 1000° C. [refs. 205, 210]

Hot Deformation of Zirconium $\alpha + \beta$ Structures

In high rate hot compression (850–970° C) of Zircaloy-2, the $\alpha + \beta$ behaves like a simple mixture composite in which each phase deforms at the same rate and develops the appropriate stress according to its power law [207,211]. With grains above 30 μm, m values are 0.2 to 0.25, with a peak in m at about 25% β which is related to formation of continuous β phase [208,209]. In Zircaloy-4 (Zr–1.4Sn–0.21Fe–0.1Cr) from 840–970° C for rates greater than $3 \times 10^{-3}\ s^{-1}$, the ($\alpha + \beta$) material has a hot work activation energy of 155 kJ/mol which is similar to β phase [202]. In Zr–2.5Nb at 85% β (875° C), the strength is about one fifth that of 85% α (725° C) and is the condition for *extrusion of pressure tubes* [212–214]. After $\alpha + \beta$ deformation in both Zircaloy-2 and Zr–2.5Nb (600–900° C), static softening occurs up to 40% by recovery in 10 s and completely by recrystallization in 600 s [215].

In specimens of Zr–2.5Nb with about 15% α in the form of *Widmanstatten plates* there is marked *flow softening* due to realignment and spheroidization of the α plates [212,215]. The relative softening is greater for thinner α plates and at lower $\dot{\varepsilon}$, with occurrence of greater spheroidization. For strain rates of $10^{-3}s^{-1}$, the value of m was 0.23 at the peak stress declining to 0.2 at $\varepsilon = 0.8$ [215]. In Zircaloy-2 with equiaxed grains, flow softening is not observed and m values lie between 0.2 for α and 0.3 for β [208]. Such flow softening is similar to that taking place in lamellar ($\alpha + \beta$) titanium alloys and in the spheroidization of pearlite.

In Zr–2.5Nb, a yield drop is found when β is a significant proportion and has a high Nb concentration due to partitioning [203,212]. The yield drop is restored by annealing/aging which re-establishes the clusters; this is enhanced by the presence of a substructure [212]. In Zircaloy-2 (Figure 17), the yield drop rises as the β fraction increases to 0.5–0.8 due to formation of $Zr(FeCr)_2$ zones [209,215].

Hot Ductility and Superplasticity

For Zircaloy-4 at $10^{-3}s^{-1}$, the elongation is 90–100% for β phase at 1200° C, declines to 65% at 900° C in $\alpha + \beta$ condition but rises to 75% at 750° C in the α phase [217]. At a rate below $10^{-4}s^{-1}$, the ductilities of α or β phase are as above, but that of $\alpha + \beta$ increased to 140% indicative of superplasticity. Zr–2.5Nb shows similar behavior with peaks of 550% and m = 0.45 in the $\alpha + \beta$ region (10^{-2} to $10^{-4}s^{-1}$) centered at 800° C (Figure 18) in the upper half of the $\alpha + \beta$ region indicating that a high proportion of soft β phase is necessary [218,219]. At the maximum ductility, the deformed material is characterized by equiaxed grains

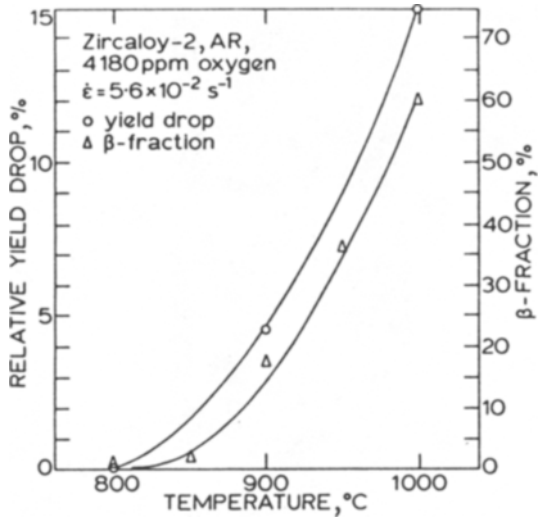

Fig. 17. Temperature dependence of the relative yield drop and beta volume fraction in Zircaloy-2. [ref. 215]

[218,219] and a flow stress minimum about 20% below that of the β phase [220]. At $\dot{\varepsilon} < 10^{-3}s^{-1}$ in Zircaloy-2, superplasticity, with m = 0.4–0.55 and Q = 57 kJ/mol, is observed in refined two phase alloys notably when β exceeds 50% [202,215–217].

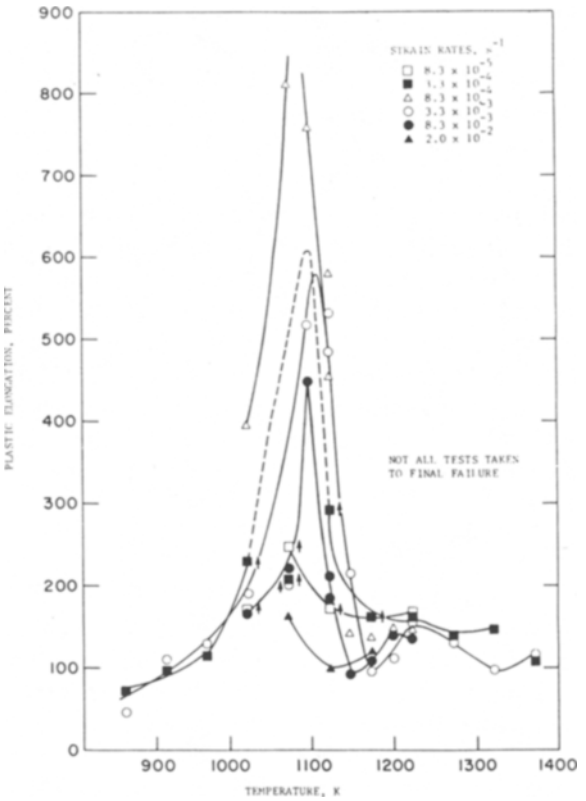

Fig. 18. Temperature and strain rate dependence of the percentage of plastic elongation for Zr–2.5Nb. [ref. 218]

BCC REFRACTORY METALS

The bcc refractory metals molybdenum (Mo), tungsten (W), niobium (Nb), and tantalum (Ta) respond to deformation similar to α iron, demonstrated by the similarity of their deformation mechanism maps, Figure 19 [27]. The structural changes associated with high temperature deformation of molybdenum involve a transition from jogged and tangled cells at high stresses and low temperatures to well-defined subgrains at low stresses and high temperature, Figure 20 [221]. The subgrain size of arc-cast molybdenum varies with stress raised to the -1 power for low stresses ($\sigma < 10^{-3}E$, subgrains) and -2 power for high stresses ($\sigma > 10^{-3}E$, cells), Figure 21. Similar stress dependence on subgrain size in ferrous metals has been reviewed by Young and Sherby [60]. Molybdenum and tungsten alloys benefit from thermomechanical treatment although little has been published on their hot working.

The importance of *substructure* in high temperature deformation of refractory metals is illustrated by Mo–5W which is given a thermomechanical treatment of swaging, recrystallizing, and variable swaging. A change in strain from 20 to 80% decreased the creep rate by a factor of 10 at 1100° C and of 40 at 1400° C. The extent of strain did not alter the subgrain size (~2 μm) but the average subboundary misorientation increased from 0.2 deg at 20% to 0.8 deg at 50% [33,222]. A similar increase in creep resistance was observed in Mo precrept over a range of T, $\dot{\varepsilon}$, and ε in which the subgrain size varied from 3.2 to 5.7 μm and the misorientation angle ω from 0.1 deg to 1.2 deg (ε = 0.1 and 0.8, $\omega = 0.411 + 0.997\varepsilon$). Rosen

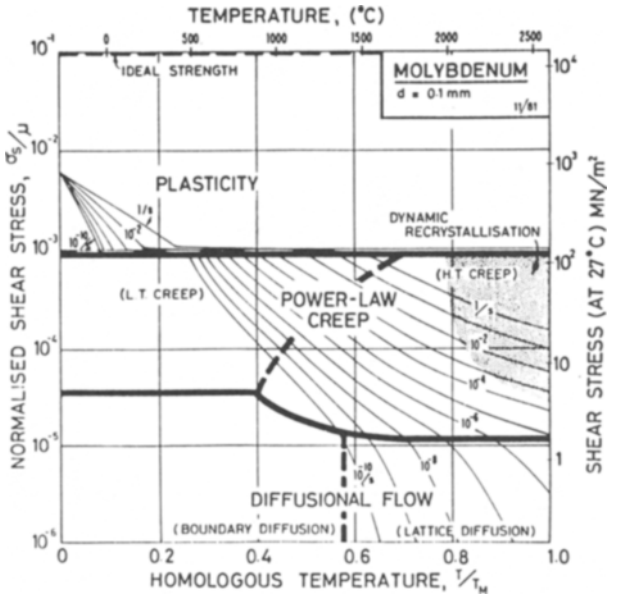

Fig. 19. A deformation map for molybdenum. [ref. 27]

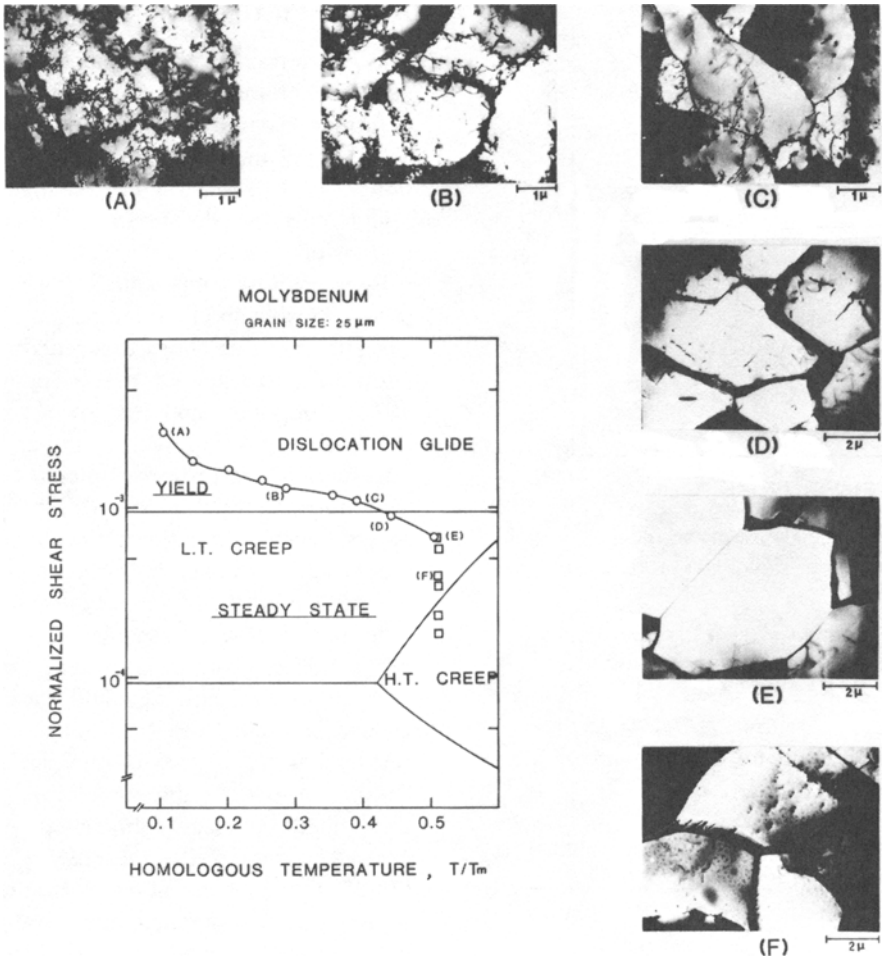

Fig. 20. The transition from cell structure to subgrain structure with increasing temperature for arc-cast molybdenum, relative to a deformation mechanism map. [ref. 221]

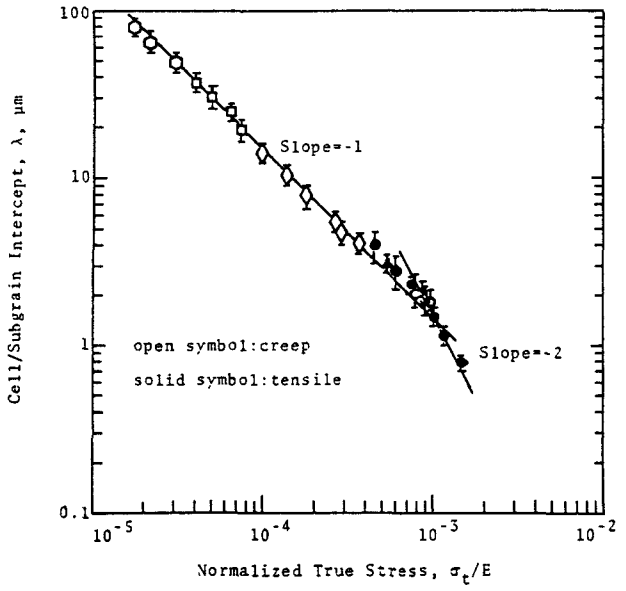

Fig. 21. A plot of cell/subgrain intercept size versus modulus-compensated true stress for arc-cast molybdenum. [ref. 221]

et al. propose a model in which only subboundaries with a misorientation exceeding a critical value contribute to strengthening. The effective subgrain size is defined by these strong subboundaries [223]. The creep resistance of molybdenum alloy TZM is also improved by thermomechanical processing [224]. The mechanism is similar to that described previously for Mo–5W. An additional effect is resolutionizing and reprecipitation of precipitates on subgrain boundaries.

CONCLUSIONS

Hot working of the bcc metals α iron, β titanium, β zirconium, and the refractory metals in the absence of recrystallization is associated with a monotonic increase in stress to a plateau value. The strain rate and temperature dependence of stress is given by the traditional power, exponential, or sinh functions of the temperature compensated strain rate, or Zener–Holloman parameter. Flow softening, which resembles dynamic recrystallization, occurs as a result of spheroidization of a second phase, conversion to a softer

texture or strain aging. The resulting structures consist of elongated grains containing an equiaxed dislocation substructure which increases in size and definition with increasing deformation temperature.

Superplasticity is found in two phase metals under specific conditions of strain rate and stress. It is associated with ferrous alloys containing 1 to 2% carbon and duplex titanium and zirconium alloys consisting of greater than 50% β.

Thermomechanical processing (TMP) of ferrous alloy centers around spheroidization of pearlite and near-net shape forming. β-Ti and β-Zr transform on cooling, so TMP produces spheroidization of $\alpha + \beta$ lamellae and cooling rate-dependent room temperature structures. The presence of substructures in β-Zr, as well as in molybdenum alloys, dramatically improves the resistance of the metals to creep.

ACKNOWLEDGMENTS

The authors wish to thank H. Oikawa, I. Weiss, N. Christodoulos and R. Choubey for reviewing portions of the manuscript. Assistance from Mr. Y. W. Kim during the early stages of manuscript preparation was very much appreciated. Support from the following funding agencies is acknowledged: NSF (DMR-8113087), NSERC Canada, and FCAR Quebec.

REFERENCES

1. H.J. McQueen and J.J. Jonas, *J. Appl. Metal Work., 3,* 1984, pp. 233–241.
2. H.J. McQueen and J.J. Jonas, *J. Appl. Metal Work., 3,* 1985, pp. 410–420.
3. W.G. McG. Tegart, *Ductility,* ASM, Metals Park, Ohio, 1968, pp. 133–177.
4. J.J. Jonas, C.M. Sellars, and W.J. McG. Tegart, *Met. Rev., 14,* 1969, pp. 1–24.
5. C.M. Sellars and W.J. McG. Tegart, *Int. Met. Rev., 17,* 1972, pp. 1–24.
6. H.J. McQueen and J.J. Jonas, *Treatise on Materials Science and Technology,* Plastic Deformation of Materials, R.J. Arsenault, ed., Academic Press, New York, 1975, Vol. 6, pp. 393–493.
7. H.J. McQueen, *Metallurgia I Oldewnictwo (Metallurgy and Foundry), 5,* 1979, pp. 421–470.
8. H.J. McQueen, *Met. Trans., 8A,* 1977, pp. 807–824.
9. H.J. McQueen, J. Sankar, and S. Fulop, *Mechanical Behavior of Materials (ICM3),* Pergamon Press, Oxford, UK, 1979, Vol. 2, pp. 675–684.
10. C.M. Sellars, *Hot Working and Forming Processes,* C.M. Sellars and G.J. Davies, eds., Metals Society, London, 1980, pp. 3–15.
11. H.J. McQueen, *Can. Met. Q., 21,* 1982, pp. 445–460.
12. J.J. Jonas and T. Sakai, *Deformation, Processing and Structure,* G. Krauss ed., ASM, Metals Park, Ohio, 1984, pp. 185–243.
13. W. Roberts, ibid, pp. 109–184.
14. H.J. McQueen and H. Mecking, *Creep and Fracture of Engineering Materials and Structures,* B. Wilshire and D.R.J. Owen eds., Pine Ridge Press, Swansea, U.K., 1984, pp. 169–184.
15. H.J. McQueen, M.G. Akben, and J.J. Jonas, *Microstructural Characterization by Non-Microscopic Techniques,* N.H. Andersen et al. eds., Riso Natl. Lab., Roskilde, Denmark, 1984, pp. 397–404.
16. W. Roberts, *Strength of Metals and Alloys (ICSMA7)* H.J. McQueen et al. eds., Pergamon Press, Oxford, U.K., 1986, Vol. 3, pp. 1859–1892.
17. H.J. McQueen and B. Baudelet, *Strength of Metals and Alloys (ICSMA5),* P. Haasen et al. eds., Pergamon Press, Oxford, 1979, Vol. 1, pp. 329–336.
18. J.N. Edington, *Met. Tech., 3,* 1976, pp. 138–153.
19. O.D. Sherby and J. Wadsworth, *Deformation, Processing and Structure,* G. Krauss, ed., ASM, Metals Park, Ohio, 1984, pp. 355–388.
20. B. Baudelet, *Proc. 4th Intl. Conf. on Strength of Metals and Alloys,* C. G'sell ed., ENSMIN, Nancy, 1976, Vol. 1, pp. 2–25.
21. D.M.R. Taplin, G.L. Dunlop, and T.G. Langdon, *Am. Rev. Mater. Sci., 9,* 1979, pp. 151–189.
22. R.C. Gifkins, *Superplastic Forming of Structural Alloys,* N.E. Paton and C.H. Hamilton, eds., Met. Soc. AIME, Warrendale, Pennsylvania, 1982, pp. 3–24.
23. A.K. Ghosh, ibid, 1982, pp. 85–104.
24. C. Hammond, ibid, 1982, pp. 131–146.
25. N. Ridley, ibid, 1982, pp. 191–203.
26. O.D. Sherby and O.A. Ruano, ibid, 1982, pp. 241–254.
27. H.J. Frost and M.F. Ashby, *Deformation Mechanism Maps,* Pergamon Press, Oxford, 1982.
28. P.M. Sargent and M.F. Ashby, *Scripta Met., 16,* 1982, pp. 1415–1422.
29. W.D. Nix and B. Ilschner, *Strength of Metals and Alloys, (ICSMA5),* P. Haasen ed., Pergamon Press, Oxford, 1979, Vol. 3, pp. 1503–30.
30. H. Mecking, *Dislocation Modelling of Physical Systems,* M.F. Ashby, ed., Pergamon Press, Oxford, 1980, pp. 197–211.
31. W. Blum, H. Munch, and P.D. Portella, *Creep and Fracture of Engineering Materials and Structures,* B. Wilshire and D.R.J. Owen eds., Pineridge Press, Swansea, U.K., 1984, Vol. 1, pp. 131–147.
32. W.D. Nix and J.G. Gibeling, *Flow and Fracture at Elevated Temperatures,* R. Raj ed., ASM, Metals Park, Ohio, 1985, pp. 1–64.
33. L. Bendersky, A. Rosen, and A.K. Mukherjee, *Int. Met. Rev., 30,* 1985, pp. 1–15.
34. J.J. Jonas, D.R. Axelrad, and J.L. Uvira, *Trans. JIM,* (supplement), 1968, pp. 257–267.
35. D.N. Hawkins, *J. Mech. Work Technol., 11,* 1985, pp. 5–21.
36. G. Glover and C.M. Sellars, *Met. Trans., 4A,* 1973, pp. 765–775.
37. G.A. Redfern and C.M. Sellars, *I.S.I. London,* S.R. #108, 1968, p. 29.
38. G.A. Redfern and C.M. Sellars, *JISI, 208,* 1970, p. 576.
39. J.L. Uvira and J.J. Jonas, *Trans. TMS-AIME, 242,* 1968, pp. 1619–1626.

40. O. Kosik, D.J. Abson, and J.J. Jonas, *JISI, 209,* 1971, pp. 624–629.
41. J.-P.A. Immarigeon and J.J. Jonas, *Acta Met., 19,* 1971, pp. 1053–1061.
42. F. Garofalo, *Fundamentals of Creep and Creep-Rupture in Metals,* MacMillan, New York, 1965.
43. K. Osakada and S. Fujii, *J. Mech. Work. Technol., 2,* 1978, pp. 241–253.
44. J.D. Embury, A.S. Keh, and R.M. Fisher, *Trans. TMS-AIME, 236,* 1966, pp. 1252–1260.
45. C.R. Barrett, W.D. Nix, and O.D. Sherby, *Trans ASM, 59* #3, 1966, pp. 3–15.
46. C. Persad, Ph.D. Thesis, University of Texas at Austin, 1983, Austin, Texas.
47. D.L. Bourell and O.D. Sherby, *Met. Trans., 12A,* 1981, pp. 140–142.
48. G. Langford and M. Cohen, *Trans ASM, 62,* 1969, pp. 623–638.
49. D.L. Bourell and O.D. Sherby, *Met. Trans., 12A,* 1981, pp. 1543–1545.
50. C.G. Schmidt, C.M. Young, B. Walser, R.H. Klundt, and O.D. Sherby, *Met. Trans., 13A,* 1982, pp. 447–456.
51. K.D. Challenger and J. Moteff, *Met. Trans., 4A,* 1973, pp. 749–755.
52. O.D. Sherby, A.K. Miller, and M.E. Kassner, *Metals Forum, 4*#1 and 2, 1981, pp. 53–56.
53. M.R. Staker and D.L. Holt, *Acta Met., 20,* 1972, pp. 569–579.
54. A.K. Mukherjee, *Treatise on Materials Science and Technology, Plastic Deformation of Materials,* R.J. Arsenault, ed., Academic Press, New York, 1975, vol. 6, p. 163.
55. C.G. Schmidt, R. Klundt, and O.D. Sherby, *Subgrain Refinement Strengthening, EY-76-5-03-0326-PA38,* USRDA, Wash. D.C., 1977.
56. M.E. Kassner, A.K. Miller, and O.D. Sherby, *Met. Trans., 13A,* 1982, pp. 1977–86.
57. H. McQueen, *Materials Technology-An Inter-American Approach,* 1968, ASME, New York, pp. 379–380.
58. R. Lombry, C. Rossard, and B.J. Thomas, *Rev. Met., 78,* 1981, pp. 975–988.
59. C. Rossard, *Metaux, Corrosion, Industries, 35,* 1960, pp. 190–205.
60. C.M. Young and O.D. Sherby, *JISI, 211,* 1973, pp. 640–647.
61. J.D. Baird and C.R. MacKenzie, *JISI, 202,* 1964, pp. 427–436.
62. J.D. Baird and A. Jamieson, *The Relation Between Structure and Properties of Metals,* (NPL Symposium), HMSO, 1963, p. 362.
63. W.C. Leslie, T.J. Michelak, and F.W. Aul, *Iron and Its Dilute Solid Solutions,* C.W. Spenser and F.E. Werner, eds., Interscience, New York, 1963, p. 119.
64. H.J. Rack and M. Cohen, *Int. J. Matl. Sci. Eng., 6,* 1970, p. 320.
65. J.D. Baird: *JISI, 204,* 1966, p. 44.
66. D.A. Hardwick and G.R. Wallwork, *ASME Publ. MPC 8,* 1978, pp. 21–29.
67. M.Kh. Shorshorov, *The Microstructure and Design of Alloys (ICSMA 3),* The Institute of Metals, London, 1973, vol. 2, pp. 43–56.
68. F.J. Torreuldea and J. Gil-Sevillano, *Strength of Metals and Alloys, (ICSMA 6),* R.C. Gifkins ed., Pergamon Press, Oxford, 1983, vol. 1, pp. 547–552.
69. M. Hatherly, ibid., vol. 3, pp. 1181–1195.
70. S. Drymek and M.R. Blicharski, *Scripta Met., 18,* 1984, pp. 99–104.
71. J.L. Lytton, *Trans. AIME, 233,* 1965, p. 1399.
72. M. Hatherly and H.S. Malin, *Scripta Met., 18,* 1984, pp. 449–454.
73. J.D. Embury and R.M. Fisher, *Acta Met., 14,* 1966, pp. 147–159.
74. D. Bourell, C. Persad, and G.A. Theriot-Giron, *Res. Mech., 12,* 1984, pp. 125–141.
75. D.L. Bourell, *Res. Mech. Ltrs., 1,* 1981, pp. 417–421.
76. C. Persad and D.L. Bourell, *Res. Mech., 16,* 1985, pp. 185–192.
77. P. Dadras, *Scripta Met., 11,* 1977, pp. 279–281.
78. D.J. Abson and J.J. Jonas, *Met. Sci. J., 4,* 1970, p. 24.
79. D.J. Abson and J.J. Jonas, *J. Nuclear Mat., 42,* 1972, p. 73.
80. H.J. McQueen and J.E. Hockett, *Met. Trans., 1,* 1970, pp. 2997–3004.
81. B.L. Bramfitt and A.R. Marder, *Processing and Properties of Low Carbon Steel,* J.M. Gray, ed., 1973, TMS-AIME, pp. 191–224.
82. O.D. Sherby, M.J. Harrigan, L. Chamagne, and C. Sauve, *ASM Trans. Quart., 62,* 1969, pp. 575–580.
83. L.A. Chojnowski and W.J. McG. Tegart, *J. Metal Sci., 2,* 1968, p. 14.
84. D.F. Lupton and D.H. Warrington, *J. Met. Sci., 6,* 1972, pp. 200–204.
85. J.L. Robbins, O.C. Sheppard, and O.D. Sherby, *JISI, 202,* 1964, pp. 804–807.
86. J.L. Robbins, O.C. Sheppard, and O.D. Sherby, *ASM Trans. Quart., 60,* 1967, p. 205.
87. M.J. Harrigan and O.D. Sherby, *Mater. Sci. Eng., 7,* 1971, pp. 177–189
88. J.L. Uvira, D.B. Clay, P.J. Worthington, and J.D. Embury, *Can. Met. Quart., 11,* 1972, pp. 439–449.
89. R. McCallum, E.S. Tweedie, and M.G. Cockcroft, *NEL Report #471,* National Engineering Laboratory, East Kilbride, Glasgow, 1970.
90. J.J. Irani and P.R. Taylor, *Deformation Under Hot Working Conditions,* SR #108, Iron and Steel Inst., London, 1968, p. 83.
91. G.F. Melloy and J.D. Dennison, *The Microstructure and Design of Alloys, (ICSMA 3),* The Institute of Metals, London, 1973, vol. 1, pp. 60–64.
92. T. Oyama, O.D. Sherby, J. Wadsworth, and B. Walser, *Scripta Met., 18,* 1984, pp. 799–804.
93. T. Chandra, D. Bendeich, and D.P. Dunne, *Strength of Metals and Alloys, (ICSMA6),* R.C. Gifkins, ed., Pergamon Press, Oxford, 1983, Vol. 1, pp. 505–510.
94. T. Chandra, D.P. Dunne, and P. Campbell, *Strength of Metals and Alloys (ICSMA7),* H.J. McQueen et al., eds., Pergamon Press, Oxford, U.K., 1986, vol. 2, pp. 947–952.

95. S.K. Srivastava and V.R. Ishawar, *New Developments in Stainless Steel Technology,* ASM, Metals Park, Ohio, 1985, pp. 187–194.
96. F.E. Al-Jouni and C.M. Sellars, *Deformation of Multi-Phase and Particle-Containing Materials,* J.B. Bilde-Sorerson, ed., Riso Natl. Labs, Roskilde, Denmark, 1983, pp. 131–137.
97. J. Ruzzante, G. Carfi, J. Torno and A.M. Hey, *Strength of Metals and Alloys, (ICSMA6),* R.C. Gifkins, ed., Pergamon Press, Oxford, 1983, Vol. 1, pp. 223–228.
98. F.E. White, *Rev. Met., 63,* 1966, pp. 991–998.
99. F.E. White and C. Rossard, *Deformation Under Hot Working Conditions,* SR #108, Iron and Steel Inst., London, 1968, pp. 14–20.
100. M.D. Coward, G.J. Richardson, and C.M. Sellars, *Met. Tech., 4,* 1977, pp. 75–80.
101. F.N. Rhines and P.J. Wray, *Trans. ASM, 54,* 1961, pp. 117–128.
102. R.A. Reynolds and W.J. McG. Tegart, *JISI, 200,*1962, pp. 1044–1059.
103. J.L. Robbins, O.C. Sheppard, and O.D. Sherby, *JISI, 199,* 1961, pp. 175–180.
104. A. Gueussier and R. Castro, *Rev. Met., 55,* 1958, pp. 1023–1040.
105. J.A. Schey, *J. Appl. Metalw., 1#2,* 1980, pp. 48–59.
106. O.D. Sherby, S. de Jesus, T. Oyama, and A.K. Miller, *Plasticity of Metals at Finite Strain: Theory, Experiment and Computation,* E.H. Lee and R.L. Mallett, eds., Stanford Press, Stanford, California 1981.
107. I.L. Dillamore and W.T. Roberts, *Met. Rev., 10* #38, 1965, pp. 271–380.
108. D.L. Bourell, Ph.D. Thesis, Stanford University, 1979, Stanford, California.
109. H. Hawkins, *Metals Tech., 3,* 1976, pp. 417–421.
110. B.L. Bramfitt and R.A. Marder, *Met. Trans., 8A,* 1977, p. 1283.
111. T. Coleman, D. Dulieu, and J.K. Gaugh, *The Microstructure and Design of Alloys, (ICSMA 3),* The Institute of Metals, 1973, London, vol. 1, p. 70.
112. R. Scholfield, G. Rosentree, N.V. Sarma, and R.T. Rainer, *Met. Tech. 1,* 1974, p. 325.
113. E. Miyoshi, Y. Ito, H. Iwanga, and T. Yamura, *Proceedings of the AWS 55th Annual Meeting,* AWS, Miami FL, May, 1974, p. 2.
114. D.N. Hawkins, *Met. Tech., 5,* 1978, pp. 37–44.
115. D.L. Bourell, *Met. Trans., 14A,* 1983, pp. 2487–2496.
116. D.L. Bourell and O.D. Sherby, *Met. Trans., 14A,* 1983, pp. 2563–2566.
117. I. Haessner and H. Weik, *Archiv. Eisen., 33,* 1962, p. 393.
118. H. Moeller and H. Staeblein, *Archiv. Eisen., 29,* 1958, p. 377.
119. J. Bennewitz, *Archiv. Eisen., 33,* 1962, p. 393.
120. D.H. Hawkins and G. Tsinopoulos, *J. Mech. Work Technol., 2,* 1978, pp. 161–177.
121. C.S. Barrett, *Structure of Metals,* McGraw-Hill, New York, 1952.
122. V.P. Gubchevskii, V.A. Zemlyanskov, D.M. Zlatoustovskii, L.D. Zlatoustovskaya, and E.D. Nemkina, *Steel U.S.S.R. 5,* 1975, pp. 276–278.
123. R.A.P. Djaic-Petkovic and J.J. Jonas, *JISI, 210,* 1972, p. 256.
124. G. Glover and C.M. Sellars, *Met. Trans., 3A,* 1972, pp. 2271–2280.
125. A.T. English and W.A. Backofen, *Trans. AIME, 230,* 1964, pp. 396–407.
126. M. Iino, *Trans ISIJ, 18,* 1978, p. 339.
127. T.G. Byrer, *SME Techn. Paper #MM75-129,* SME, Dearborn, Michigan, 1975.
128. M. Hirschvogel, *J. Mech. Work. Technol., 2,* 1979, pp. 317–332.
129. A.G. Mamalis, *J. Mech. Work. Technol., 5,* #1–2, 1981, pp. 69–84.
130. B. Avitzur and L. Ache, *Prec. Met., 3*#12, 1980, pp. 21–23.
131. R.W. Pollard and L.L. Stalnaker, *Tool Prod., 47,* 1981, pp. 88–89.
132. B.A. MacKenzie, *Mech. Des., 53,* 1981, pp. 131–134.
133. T.A. Dean and C.E.N. Sturgess, *J. Mech. Work. Technol.,* 2 #3, 1978, pp. 255–265.
134. A.W. Hughes, K.A. Lane, and S. Orman, *J. Nucl. Mat., 48,* 1973, pp. 172–182.
135. T.A. Dean and C.R. Anderton, *Int. J. Mach., 14,* 1974, pp. 1–12.
136. H. Diether, *J. Mech. Work. Technol., 2,* 1978, pp. 205–215.
137. S.E. Rogers, *Metall. Met. Form., 43,* 1976, pp. 36–39.
138. A.A. Popoff and J.R. Becker, *Met. Eng. Quart., 12,* 1972, pp. 21–29.
139. B. Appell, *J. Mech. Work. Technol., 2,* 1978, pp. 197–203.
140. P. Mullins, *Iron Age Metalwork Int., 16,* 1977, pp. 19–20.
141. N. Yamagoshi, T. Minami, and S. Aihora, *Wire Journal,* Oct. 1973, pp. 68–81.
142. K. Yuasa, *Metall. Met. Form., 41,* 1974, pp. 164–171.
143. S.K. Samanta, *Int. J. Mech. Sci., 10,* 1968, pp. 613–636.
144. M. Burgdorf, *Metall. Met. Form., 38,* 1971, pp. 76–79.
145. B. Orrling, *Jernkontorets Ann., 161,* 1977, pp. 104–108.
146. P.F. Thomason, *Proc. Instr. Mech. Engrs., 184,* 1969–70, pp. 885–895.
147. I. Gokyu, T. Kishi, and M. Ogura, *JIIM, 32,* 1963, pp. 289–294.
148. E.J. Ripling and R.S. Lindberg, *J. Basic Engr., 87* #2, 1965, pp. 307–312.
149. R. El-Koussy and V.P. Polukhia, *J. Mech. Work. Technol., 2,* 1978, pp. 145–160.
150. M. Page, *IAMI, 19,* 1980, pp. 37–39.
151. O.D. Sherby, B. Walser, C.M. Young, and E.M. Cady, *Scripta Met., 9,* 1975, p. 569.
152. B. Walser and O.D. Sherby, *Met. Trans., 10A,* 1979, pp. 1461–1471.
153. J. Wadsworth and O.D. Sherby, *J. Mech. Work. Technol., 2,* 1978, pp. 53–66.
154. T. Itoh, M. Tokizane, J. Wadsworth, and O.D. Sherby,

J. Mech. Work. Technol., 5, 1981, pp. 105–123.
155. I. Gokyo and T. Kishi, (ICSMA 1); *JJIM, 32,* 1968, pp. 177–181.
156. I. Gokyo, T. Kishi, and M. Ogura, *JJIM, 31,* 1967, pp. 357–362.
157. M. Azrin, G.B. Olson, and R.A. Gagne, *Met. Sci. Eng., 40,* 1978, pp. 175–185.
158. M.R. Krishnadev, I. Le May, and A. Galibois, *Trans. ISIJ, 14,* 1974, pp. 369–371.
159. C.M. Young, B. Walser, E.P. Abrahamson, and O.D. Sherby, *Scripta Met., 9,* 1975, pp. 35–38.
160. K. Yuasa and Y. Murata, *Metall. Met. Form., 41,* 1974, pp. 290–294.
161. I.N. Bogachev, T.D. Eysmondt, and A.V. Fugman, *Phys. Met. Metallog., 34,* 1972, pp. 126–133.
162. I. Gokyu and K. Hashimoto, *JJIM, 31,* 1967, pp. 580–584.
163. I. Gokyu, T. Kishi, and M. Ogura, *JJIM, 32,* 1968, pp. 202–207.
164. T. Hashimoto, T. Sawandra, and H. Ohtani, *Tetsu-to-Hagone, 65,* 1979, pp. 1425–1433.
165. G. Baldi and G. Buzzichelli, *Met. Sci. 12,* 1978, pp. 459–472.
166. A.J. McEvily and K.H. Bush, *Trans. ASM, 55,* 1962, p. 654.
167. T. Terazawa, H. Higashiyama, and S. Sekino, *Towards Improved Ductility and Toughness,* Kyoto Int. Conf., BISI Translation 10937, 1971, p. 101.
168. S.D. Dabkowski, P.J. Korkol, and M.F. Baldy, *Met. Eng. Q., 16,* 1976, pp. 22–32.
169. H. Hero, J. Evensen, and J.D. Embury, *Can. Met. Quart., 14,* 1975, p. 117.
170. I. Koyasu and H. Kubota, *Trans. ISIJ, 11,* 1971, p. 321.
171. M. Iino, H. Mimura, and N. Nomura, *Trans. ISIJ, 17,* 1977, p. 450.
172. W.B. Morrison, *Met. Tech., 2,* 1975, p. 33.
173. P. Griffiths and C. Hammond, *Titanium Science and Technology,* Plenum Press, New York, 1973, pp. 1155–1167.
174. R.E. Lewis, I.L. Caplan, and W.C. Coons, *Creep and Fracture of Engineering Materials and Structures,* B. Whilshire and D. Owen eds. Pineridge Press, Swansea, U.K., 1984, pp. 433–450.
175. R.E. Lewis, W.C. Coons, and I.L. Caplan, ibid, pp. 419–431.
176. H. Oikawa and M.X. Cui, *Strength of Metals and Alloys, (ICSMA 7),* H.J. McQueen et al. eds., Pergamon Press, Oxford, 1986, Vol. 1, pp. 601–606.
177. H. Oikawa, K. Nishimura, and M.X. Cui, *Scripta Met. 19,* 1985, pp. 825–828.
178. H. Oikawa, *Scripta Met. 19,* 1985, pp. 1351–1354.
179. J.J. Jonas and J.P. Immarigeon, *Z. Metall. 60,* 1969, pp. 227–231.
180. C.G. Shelton and B. Ralph, *Scripta Met. 19,* 1985, pp. 407–418.
181. I. Weiss, G.E. Welsch, F.H. Froes, and D. Eylon, *Titanium Science and Technology,* Proc. 5th Intnl. Conf. on Titanium, 1984, pp. 1503–1510.
182. C. Hammond and J. Nutting, *Met. Sci., 11,* 1977, pp. 474–477; *Forging and Properties of Aerospace Materials,* Metals Society, London, 1978, pp. 75–102.
183. F.J. Gurney and A.T. Male, *Titanium Science and Technology,* Plenum Press, New York, 1973, pp. 1769–1784.
184. F.A. Crosseley, R.L. Boorn, R.W. Lindberg, and R.E. Lewis, ibid, pp. 2025–2039.
185. I. Weiss and H. Froes, *Titanium Science and Technology,* Proc. 5th Intnl. Conf. on Titanium, 1984, pp. 499–506.
186. I. Weiss, F.H. Froes, and P.J. Bania, *Strength of Metals and Alloys, (ICSMA 7),* H.J. McQueen et al., eds., Pergamon Press, Oxford, 1986, Vol. 2, pp. 1055–1061.
187. J.E. Coyne, *Forging and Properties of Aerospace Materials,* Metals Society, London, 1978, pp. 234–247.
188. J.C. Williams and E.A. Starke, *Deformation, Processing and Structure,* G. Krauss ed., ASM Metals Park, Ohio, 1984, pp. 279–354.
189. M. Peters and G. Lutjering, *Titanium '80 Science and Technology (4th Intnl. Conf. on Ti),* H. Kimura and O. Izumi eds., AIME, Warrendale, Pennsylvania, 1980, pp. 925–935.
190. C.C. Chen and J.E. Coyne, *Met. Trans., 7A,* 1976, pp. 1931–1941.
191. A.L. Hoffmanner, *Metal Forming: Interrelation Between Theory and Practice,* A.L. Hoffmanner ed., Plenum Press, New York, 1971, pp. 349–391.
192. S.L. Semiatin and G.D. Lahoti, *Met. Trans. 12A,* 1981, pp. 1705–1717.
193. S. Gautron, J.P. Immarigeon, and G. L'Esperance, *Strength of Metals and Alloys, (ICSMA 7),* H.J. McQueen et al., eds., Pergamon Press, Oxford, 1986, vol. 2, pp. 1067–1072.
194. I. Weiss, G.E. Welsch, F.H. Froes and D. Eylon, ibid., pp. 1073–1079.
195. F.H. Froes, C.F. Yolton, J.C. Chesnutt, and C.H. Hamilton, *Forging and Properties of Aerospace Materials,* Metals Society, London, 1978, pp. 371–398.
196. G.W. Greenwood, W.E. Seeds, and S. Yure, ibid., pp. 253–265.
197. A.K. Ghosh and C.H. Hamilton, *Met. Trans., 10A,* 1979, pp. 699–706.
198. A. Arieli and H. Rosen, *Met. Trans., 8A,* 1977, pp. 1591–1596.
199. P. Dadras, J.F. Thomas, and J.C. Moosbrugger, *Met. Trans. 14A,* 1983, pp. 1512–1516.
200. D. Lee and W.A. Backofen, *Trans. AIME, 239,* 1967, pp. 1034–1040.
201. W.A. Reinsch and H.W. Rosenberg, *Met. Progress. 117#4,* 1980, pp. 64–69.
202. H.E. Rosinger, P.C. Bera, and W.R. Clendening, *J. Nucl. Matl., 82,* 1979, pp. 286–297.
203. H. Buhler and H.W. Wagener, *Z. Metallkde, 58,* 1967, pp. 136–144.
204. B. Heritier, M.J. Luton, and J.J. Jonas, *Met. Sci., 8,* 1974, pp. 41–48.
205. J.J. Jonas, B. Heritier, and M.J. Luton, *Met. Trans. 10A,* 1979, pp. 611–620.
206. M.J. Luton and J.J. Jonas, *Can. Met. Q., 11,* 1972, pp. 79–90.
207. A.S. Rizkalla, R.A. Holt, and J.J. Jonas, *Zirconium*

in the Nuclear Industry IV, STP 681, ASTM, Philadelphia, 1980, pp. 497–513.
208. R. Choubey, J.J. Jonas, R.A. Holt, and C.E. Ells, *Zirconium in the Nuclear Industry V, STP 754,* ASTM Philadelphia, 1982, pp. 350–369.
209. R. Choubey, J.J. Jonas, and B.A. Cheadle, *Met. Trans., 13A,* 1982, pp. 1957–1964.
210. B. Heritier and J.J. Jonas, *Met. Trans, 10A,* 1979, pp. 557–567.
211. R.A. Holt anad H.E. Sills, *ANS Trans. 27,* 1977, p. 295.
212. A.S. Rizkalla, R. Choubey, and J.J. Jonas, *Zirconium in the Nuclear Industry VI, STP824,* ASTM, Philadelphia, 1984, pp. 176–179.
213. B.A. Cheadle, *Zirconium in the Nuclear Industry III, STP 633,* ASTM, Philadelphia, 1977, pp. 457–485.
214. B.A. Cheadle, S.A. Aldridge, and C.E. Ells, *Can. Met. Q., 11,* 1972, pp. 121–127.
215. R. Choubey and J.J. Jonas, *Met. Sci., 15,* 1981, pp. 30–38.
216. C.E.L. Hunt and D.E. Foote, *Zirconium in the Nuclear Industry III, STP 633,* ASTM, Philadelphia, 1977, pp. 50–56.
217. C. Peterson, *Literature Search on Properties of Zircaloy-4 at High Temperature,* (Report KFK-Ext 6/73-6, 1973), Translation AECL-5101, Atomic Energy of Canada, Mississauga, Ontario, Canada, 1973.
218. H.E. Rosinger and A.E. Unger, *Superplastic and Strain Rate Dependent Plastic Flow of Zr–2.5Nb Between 873 to 1373° K.* AECL-6418, Atomic Energy of Canada, Pinawa, Manitoba, 1979.
219. K. Nuttal, *Scripta Met., 10,* 1976, p. 833.
220. B.A. Cheadle, S.A. Aldridge, and C.E. Ells, *Effect of Deformation Temperature on Texture of Zirconium Alloy Rolled Sheet and Extruded Tubes,* AECL-3372, Atomic Energy of Canada, Chalk River, Ontario Canada, 1969.
221. K-J.F. Lee, Ph.D. Thesis, University of Cincinnati, 1980, Cincinnati, Ohio.
222. E. Freund, D. Agronov, and A. Rosen, *Strength of Metals and Alloys (ICSMA7),* H.J. McQueen et al., eds., Pergamon Press, Oxford, U.K., 1986, Vol. 1, pp. 647–652.
223. A. Rosen, L. Bendersky, and Y. Komen, *Deformation of Polycrystals,* N. Hansen et al., eds., Riso Nat'l Lab, Roskilde, Denmark, 1981, p. 351.
224. D. Agronov, E. Freund, and A. Rosen, *ibid.,* pp. 695–700.